Journal of Sustainable Development and Policy

Volume: 12; **Issue:**12
Pages: 01-51

Finite Element-Based Thermomechanical Optimization of Pressure Components for Extending Industrial Boiler Service Life

Syed Feroz Ahmed[1]; Shabbir Ahamed[2]

[1]. *Piping QC Inspector, Tanajib Gas Plant Projects, Saudi Arabia; Email: bdferoz@gmail.com*
[2]. *Mechanical Engineer, Accelleron Industries, Dhaka, Bangladesh; Email: shabbir04kuet@gmail.com*

Doi: 10.63125/x24pht28
Received: *15 September 2022;* ***Revised:*** *12 October 2022;* ***Accepted:*** *05 November 2022;* ***Published:*** *02 December 2022*

Abstract

Industrial boiler pressure components are subjected to combined internal pressure, elevated temperature, transient thermal gradients, cyclic loading, material aging, and progressive wall loss, which can accelerate creep-fatigue damage and reduce structural service life. This study developed and quantitatively evaluated a finite element-based thermomechanical optimization framework for assessing structural performance and extending the remaining service life of industrial boiler pressure components. The analysis included 216 finite element component models and 1,296 completed thermomechanical simulation cases representing headers, cylindrical pressure sections, nozzle-to-shell intersections, branch connections, and welded critical regions. The evaluated components operated at a mean pressure of 13.72 MPa and temperature of 487.6°C, with mean accumulated service exposure of 82,460 hours and wall-thickness loss of 11.8%. Baseline analysis produced a mean maximum thermal gradient of 47.6°C, equivalent stress of 286.4 MPa, strain range of 0.318%, creep damage of 0.314, fatigue usage of 0.382, and combined creep-fatigue damage of 0.527. Nozzle intersections generated the highest localized equivalent stress at 331.8 MPa. Optimization of transition geometry, local wall thickness, reinforcement, operating temperature, and transient heating and cooling conditions reduced thermal gradient by 23.9%, equivalent stress by 15.6%, strain range by 18.6%, creep damage by 26.1%, fatigue usage by 28.3%, and combined damage by 28.7%. Consequently, predicted allowable cycles increased by 35.7%, remaining allowable cycles increased by 51.7%, and mean remaining operating life increased from 71,860 to 96,740 hours, representing a 34.6% extension. Baseline-to-optimized differences were statistically significant at $p < .001$, with effect sizes reaching $d = 0.86$ for combined damage and $d = 0.87$ for remaining life. Numerical validation achieved $R^2 = .987$ for temperature and $R^2 = .972$ for equivalent stress, with principal validation deviations below 5%. The findings demonstrated that integrating finite element analysis, service-aged material behavior, operational history, creep-fatigue assessment, statistical validation, and multi-objective optimization provided a robust quantitative framework for reducing thermomechanical damage and supporting condition-informed service-life management of industrial boiler pressure components.

Keywords

Thermomechanical Optimization, Finite Element Analysis, Industrial Boilers, Creep-Fatigue Damage, Service-Life Extension.

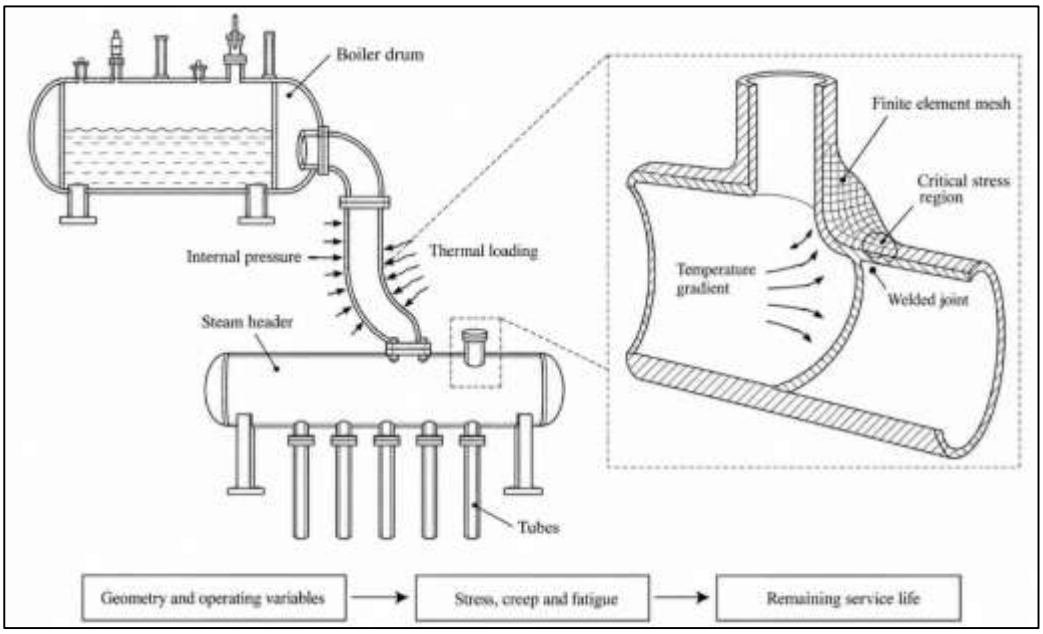
INTRODUCTION

Finite element-based thermomechanical optimization can be defined as a computational engineering approach in which finite element analysis is integrated with thermal, mechanical, material, geometric, and operational variables to identify structural configurations and operating conditions that reduce damaging stresses, strains, temperature gradients, deformation, creep, fatigue, and related failure mechanisms in engineering components (Duda & Konieczny, 2019). Within industrial boiler systems, pressure components are load-bearing structures that contain pressurized water, steam, or other working fluids while operating under elevated and often spatially nonuniform temperatures. These components commonly include boiler drums, steam headers, superheater and reheater headers, pressure vessels, tubes, piping systems, elbows, tees, nozzles, manifolds, valves, welded joints, and connecting sections. Thermomechanical behavior describes the coupled structural response generated when mechanical loads such as internal pressure, external forces, dead weight, piping reactions, and constraint forces act simultaneously with thermal loads caused by heating, cooling, temperature gradients, thermal expansion, and transient operating cycles. Service life refers to the period or number of operating cycles during which a component can continue performing its intended pressure-retaining and structural functions while maintaining acceptable integrity against specified failure mechanisms. Finite element analysis provides a numerical framework for discretizing complex pressure-component geometries into interconnected elements through which temperature, displacement, strain, stress, and time-dependent material responses can be calculated under defined boundary and loading conditions. Research across pressure-vessel engineering, power-generation equipment, high-temperature piping, boiler drums, headers, valves, welded joints, and other elevated-temperature structures has established finite element methods as important tools for resolving localized stress and temperature fields that simplified analytical procedures may not represent adequately (Ševeček et al., 2018). Studies have incorporated elastic, elastic-plastic, creep, cyclic plasticity, fatigue, creep-fatigue interaction, fracture, and coupled thermal-structural models to represent different stages of component degradation. Computational assessment has also increasingly connected operating histories with material-temperature relationships, pressure transients, heat-transfer coefficients, geometric discontinuities, and local stress concentrations. Design-by-analysis frameworks similarly employ detailed stress analysis to examine failure modes such as plastic collapse, local failure, buckling, and cyclic damage. In boiler applications specifically, finite element calculations have been applied to drums, headers, piping, valve bodies, nozzle intersections, and other critical regions to determine how temperature and pressure histories produce localized structural demand. Research on supercritical boiler pressure-reducing valves has additionally demonstrated the relevance of temperature-dependent material properties and coupled thermomechanical loading when evaluating creep-cyclic plastic behavior (Trzepieciński, 2020). Collectively, more than thirty studies across high-temperature structural integrity, pressure-vessel design, creep-fatigue assessment, remaining-life evaluation, thermal-stress analysis, and numerical optimization provide the methodological foundation for treating boiler service-life management as a coupled thermomechanical problem rather than as an isolated pressure or temperature problem.

Industrial boilers constitute critical thermal-energy infrastructure across electricity generation, petroleum refining, petrochemical processing, chemical production, pulp and paper manufacturing, food processing, metals production, district heating, pharmaceuticals, and numerous other energy-intensive industries. Their pressure-retaining components operate under conditions in which high temperature, elevated pressure, cyclic start-up and shutdown, load variation, prolonged steady operation, water and steam chemistry, vibration, and structural constraint can occur simultaneously (Sairajan et al., 2016). Consequently, maintaining boiler pressure-component integrity has international significance because degradation can affect worker safety, plant availability, energy production, maintenance expenditure, asset utilization, and continuity of industrial processes. Large fleets of conventional thermal power plants and process-industry steam systems contain components that have accumulated extensive operating hours and repeated thermal cycles, making quantitative assessment of accumulated damage central to continued operation. The engineering challenge is especially important for thick-walled components because the inner and outer surfaces may experience different heating and cooling rates during transients, producing temperature gradients that generate substantial

thermal stresses even when internal pressure remains within its permitted range. Boiler headers and high-energy piping operating under high temperature and pressure have been identified in earlier research as components exposed to interacting degradation mechanisms, including creep, fatigue, and creep-fatigue damage.

Figure 1: Thermomechanical optimization of boiler components



Operational monitoring research has therefore incorporated process variables such as steam temperature, steam pressure, steam flow, component temperature, stress history, and accumulated usage factors into structural integrity assessment. International engineering practice also relies on established pressure-equipment and fitness-for-service philosophies that evaluate allowable stresses, cyclic loading, high-temperature behavior, creep, fatigue, crack-like defects, and remaining life (Sekar et al., 2019). ASME-based high-temperature assessment literature, for example, addresses creep and creep-fatigue behavior and provides methods for evaluating pressure components operating within the creep regime. The international importance of such assessments increases when existing assets are required to operate under more variable duty, because start-ups, shutdowns, load ramps, and temperature changes can generate repeated thermal transients at geometrical discontinuities. Supercritical and other high-temperature boiler technologies further expose structural components to material-property degradation and time-dependent deformation. Studies of power-plant pressure components, pressure-reducing valves, high-temperature piping, boiler drums, and header systems have repeatedly treated structural integrity as a combined safety and economic concern. Finite element-based evaluation is particularly relevant in this international context because pressure components differ in dimensions, material grades, weld configurations, operating histories, restraint conditions, and thermal environments (Harris et al., 2019). A numerical model can incorporate these component-specific characteristics while calculating spatially resolved temperature and stress fields. This capacity permits quantitative comparison of critical regions and loading scenarios within a common mechanical framework, which is essential when industrial boiler fleets encompass different ages, capacities, manufacturers, operating regimes, and material systems.

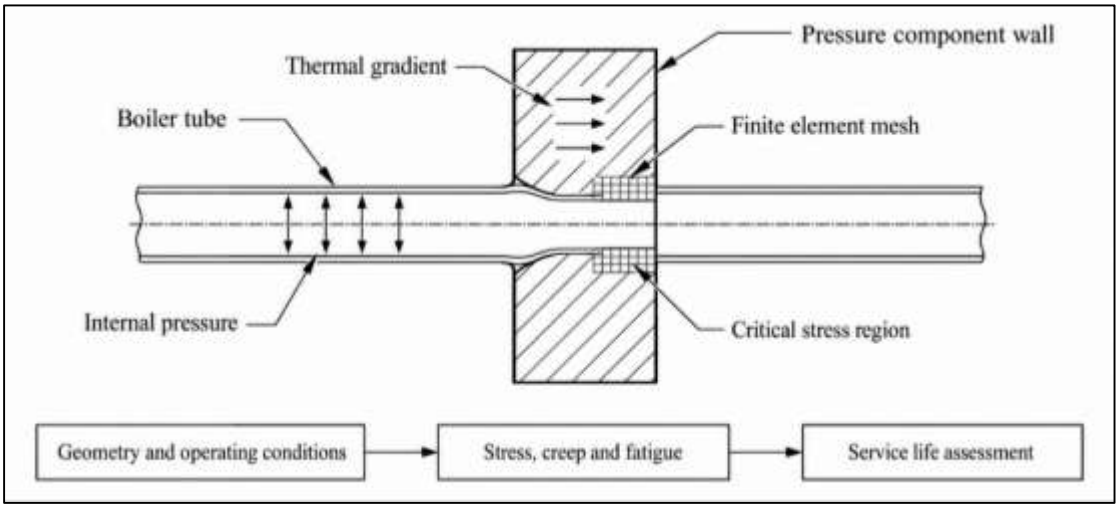
The structural condition of boiler pressure components is governed by interactions among mechanical stress, thermal stress, material response, geometry, operating duration, and loading history. Internal pressure produces membrane and bending stresses in shells, pipes, headers, drums, and junctions, while temperature gradients create thermal expansion incompatibilities that can generate additional secondary stresses. These effects become particularly important near nozzles, branch connections, welded joints, changes in wall thickness, bends, supports, penetrations, and other geometric

discontinuities where stress concentration develops (Klimiec et al., 2020). During boiler start-up, component surfaces exposed to rapidly changing steam or water temperatures may expand or contract more quickly than material farther through the wall thickness, producing transient thermal gradients. Shutdown and load-reduction events can reverse these gradients and alter the sign and magnitude of thermal stresses. Repeated cycling can progressively consume fatigue resistance, while sustained operation at elevated temperature can generate creep strain and time-dependent microstructural degradation. When cyclic thermal-mechanical loading occurs within a temperature regime where creep is significant, creep and fatigue may interact rather than developing independently. Numerical studies of high-temperature pressure components have therefore evaluated creep-fatigue interaction, cyclic plasticity, strain accumulation, stress relaxation, and deformation under realistic loading sequences. Research on supercritical boiler valves, for example, has used finite element models with temperature-dependent material properties to determine critical loading components associated with creep deformation and cyclic damage (Kim et al., 2019). Earlier investigations of power-plant components have similarly converted plant transients into temperature and stress responses and calculated fatigue and creep damage from operating histories. Welded regions introduce further complexity because base metal, weld metal, and heat-affected zones can possess different mechanical and creep properties, while manufacturing processes can generate residual stresses that remain superimposed on operational stresses. Finite element studies of pipework joints have demonstrated the value of representing manufacturing history together with through-life creep-fatigue damage and defect assessment when evaluating service integrity. Material aging, oxidation, corrosion, wall thinning, creep cavitation, thermal fatigue cracking, and crack propagation can additionally modify the effective structural capacity of pressure-retaining components. Fatigue-oriented research has shown that material properties, temperature, stress, pressure, geometry, manufacturing processes, loading history, vibration, and displacement conditions can all influence cyclic life. The resulting degradation process is therefore multivariable and spatially nonuniform. A location experiencing the highest pressure-induced membrane stress may not necessarily correspond to the location experiencing the greatest thermal stress range, creep strain, fatigue damage, or combined life consumption (Lyubimova et al., 2017). Quantitative thermomechanical analysis is consequently required to resolve these competing mechanisms and determine which combinations of temperature, pressure, geometry, material behavior, and operational cycling control the service-life consumption of specific boiler components.

Finite element analysis provides a computational basis for quantifying the spatial and temporal response of boiler pressure components under coupled thermal and mechanical loading. A typical thermomechanical assessment begins with geometric representation of the component, selection of element types and mesh density, definition of temperature-dependent material properties, specification of heat-transfer and mechanical boundary conditions, and application of pressure-temperature histories corresponding to operating conditions (Kumar et al., 2016). Thermal analysis can determine transient temperature distributions through the component wall and around discontinuities, after which the resulting temperature field can be transferred to a structural model for calculation of thermal expansion, displacement, elastic or inelastic strain, and stress. Mechanical loads including internal pressure, self-weight, external piping loads, support reactions, and contact conditions can be incorporated simultaneously. Mesh refinement is particularly important around stress-concentration regions, and published boiler-drum analysis has emphasized grid-independence verification as a prerequisite for credible numerical results. Finite element methods can also accommodate temperature-dependent elastic modulus, thermal expansion coefficient, thermal conductivity, specific heat, yield behavior, creep parameters, cyclic plasticity parameters, and other material characteristics required for high-temperature analysis. Earlier studies have used such models to investigate thick pipes, shell-nozzle junctions, boiler drums, valves, headers, welded pipework joints, and other pressure-retaining structures. Online monitoring research has extended the same principle by converting measured plant process transients into finite element-derived temperature and stress histories and subsequently evaluating accumulated creep, fatigue, and creep-fatigue usage (dos Santos et al., 2018). Finite element-based creep-fatigue tools have also employed local stress, elastic strain range, and temperature extracted from numerical models to estimate allowable loading cycles and damage interaction under

elevated-temperature service. Advanced methods include direct cyclic analysis, linear matching methods, elastic-plastic analysis, reference-stress procedures, fracture-mechanics approaches, and extended finite element formulations for crack propagation. Review research on fatigue-crack simulation further documents the use of extended finite element methods for representing crack growth without requiring conventional remeshing around every incremental crack extension. These numerical capabilities are particularly relevant to industrial boiler pressure components because local thermomechanical fields are strongly affected by geometry and boundary conditions. A nominal pressure and bulk steam temperature provide only global operating measures and cannot independently describe the localized stress-strain state at a nozzle corner, weld toe, header ligament, branch intersection, or thick-wall transition. Quantitative finite element assessment therefore transforms operational variables into local structural-response variables that can be evaluated against fatigue, creep, deformation, fracture, and code-based acceptance criteria. This relationship between measurable operating conditions and local material response forms the computational foundation for service-life-oriented thermomechanical optimization (Assefinejad et al., 2020).

Figure 2: Thermomechanical optimization of boiler components



Thermomechanical optimization extends conventional finite element assessment by treating structural response as a function that can be systematically improved through modification of design or operating variables. In pressure-component engineering, optimization variables may include wall thickness, nozzle geometry, transition radius, branch dimensions, reinforcement configuration, fillet radius, local thickness distribution, material grade, weld arrangement, support condition, insulation characteristics, heating rate, cooling rate, pressure ramp, temperature ramp, dwell time, and operating sequence. Quantitative optimization can examine how changes in these variables affect maximum temperature gradient, peak equivalent stress, principal stress, strain range, plastic strain, creep strain, fatigue usage, creep damage, deformation, and predicted service life. This approach is particularly suitable for boiler components because increasing thickness does not always reduce every damage mechanism (Pástor et al., 2020). A thicker wall may lower some pressure stresses while increasing through-wall temperature differences during rapid transients, thereby modifying thermal stress. Similarly, geometric reinforcement can reduce one local stress concentration while shifting structural demand toward an adjacent region. Optimization therefore requires simultaneous consideration of thermal and mechanical behavior rather than independent minimization of individual variables. Previous pressure-vessel and high-temperature structural research has established the usefulness of design-by-analysis procedures for evaluating primary-load capacity, strain limits, cyclic loading, and creep-fatigue damage using computational models. Studies of boiler drums have applied finite element stress and temperature analysis to determine fatigue life under cyclic steam-supply conditions, while studies of supercritical boiler valves have conducted parametric analyses to examine how changes in critical loading magnitudes influence creep and total deformation per cycle (Schiro et al., 2020). High-

temperature structural research has also developed life-diagram and direct-analysis approaches that incorporate low-cycle fatigue and creep-fatigue mechanisms under cyclic loading. Across these studies, parameter sensitivity emerges as an essential quantitative issue because structural life depends on interacting variables rather than a single maximum stress value. Optimization algorithms can be coupled with finite element simulations to search combinations of variables, while response-surface models, design-of-experiments methods, sensitivity analysis, surrogate models, and statistical regression can reduce the computational burden when large parameter spaces are examined. For service-aged boiler equipment, the optimization problem can additionally incorporate existing wall thickness, accumulated operating hours, prior thermal cycles, measured material properties, known defects, and inspection results (Kim et al., 2020). Such a formulation distinguishes life-extension analysis from greenfield component design because the initial structural state is no longer assumed to be undamaged. The quantitative framework therefore centers on determining how controllable geometric, material, and operating parameters alter local thermomechanical responses and accumulated damage within realistic structural and operational constraints.

Extending the service life of industrial boiler pressure components requires quantitative representation of accumulated damage and remaining structural capacity rather than reliance solely on chronological age. Two components installed at the same time may possess different remaining lives because their pressure histories, temperature histories, start-stop cycles, ramp rates, dwell periods, material conditions, repairs, and local stress states can differ substantially. Remaining-life assessment therefore combines information about operational exposure with models of material degradation and structural response. For components operating within the creep regime, sustained stress and temperature determine time-dependent damage, while repeated thermal and pressure transients contribute to fatigue usage (Najjar et al., 2020). Their interaction can become a controlling mechanism when elevated-temperature dwell periods and cyclic loading occur together. Published monitoring systems for high-temperature power-plant components have evaluated creep and fatigue usage continuously using measured steam pressure, temperature, and flow together with finite element-derived material temperature and stress histories. Earlier online fatigue-creep monitoring research likewise transformed plant transients into thermal and structural responses and calculated fatigue usage through cycle-counting procedures while evaluating creep damage from stress-temperature histories and material rupture relationships. ASME-oriented literature addresses remaining-life methodologies for boiler and pressure-vessel components in the creep range and treats creep-fatigue analysis as a central element of elevated-temperature structural assessment. Finite element models used for such decisions require verification because predicted life can be sensitive to mesh density, thermal boundary conditions, heat-transfer assumptions, material constitutive parameters, stress concentration, load sequence, and damage model selection. Quantitative reliability therefore involves mesh-convergence assessment, comparison with analytical solutions where applicable, validation against measured temperatures or strains, sensitivity analysis, uncertainty evaluation, and comparison of alternative constitutive or damage formulations. Experimental strain measurements, thermocouple data, nondestructive inspection results, metallurgical observations, hardness measurements, dimensional inspection, and historical operating records can provide independent information for evaluating numerical credibility (Saad et al., 2019). Studies involving manufacturing-history simulation have also shown that residual stresses and through-life operating histories can influence predicted integrity and defect tolerance, indicating that model initialization can materially affect service-life estimates. Statistical treatment is valuable when several uncertain parameters are considered because deterministic single-value inputs may conceal variability in material strength, creep properties, heat-transfer coefficients, wall thickness, operating transients, and measured loads. A quantitative service-life framework can therefore distinguish nominal predictions from ranges of plausible structural response while identifying variables that contribute most strongly to prediction uncertainty (Rouse et al., 2018). This combination of finite element simulation, operating-history reconstruction, damage assessment, verification, and parameter sensitivity provides the analytical structure required for evaluating service-aged pressure components under realistic thermomechanical conditions.

The accumulated research base demonstrates extensive development in finite element stress analysis,

transient heat transfer, fatigue evaluation, creep modeling, creep-fatigue interaction, fracture assessment, design-by-analysis, online condition monitoring, and remaining-life calculation for high-temperature pressure equipment. More than thirty studies distributed across these interconnected areas have examined individual aspects of structural integrity using boiler drums, headers, valves, pressure vessels, piping systems, welded joints, nozzle intersections, thick pipes, and other high-temperature components as analytical or experimental subjects (Trampus, 2019). A recurring characteristic of this literature is the use of detailed numerical models to identify localized structural responses that cannot be represented adequately through nominal pressure and temperature alone. Another recurring characteristic is the dependence of damage on interacting variables, including thermal gradients, mechanical loading, material temperature, hold time, geometry, cycling frequency, manufacturing history, residual stress, and time-dependent material behavior. Research on real-time monitoring has connected plant process measurements to creep and fatigue usage, boiler-drum studies have combined thermal and structural analysis with fatigue-cycle assessment, pressure-reducing-valve studies have evaluated creep-cyclic plasticity under coupled thermomechanical loading, and pipework-joint research has represented manufacturing history and operational creep-fatigue damage within detailed finite element models. Design-by-analysis research has further emphasized computational assessment of primary loading, strain limits, and creep-fatigue damage, while recent high-temperature structural studies have developed numerical life-assessment methods that consider interacting low-cycle-fatigue and creep-fatigue mechanisms (Singh et al., 2020). These streams of evidence establish a broad technical foundation, yet they also illustrate the multidimensional nature of boiler life assessment: thermal analysis alone does not quantify mechanical integrity, static stress analysis does not describe cyclic damage, fatigue assessment alone may omit sustained high-temperature degradation, and remaining-life estimation without optimization does not directly identify combinations of controllable variables associated with lower damage accumulation. The quantitative research problem is therefore centered on integrating transient thermal analysis, structural stress-strain evaluation, temperature-dependent material behavior, creep and fatigue damage, geometric parameters, operational parameters, and numerical optimization within a unified finite element framework. Such integration permits systematic measurement of relationships between input variables and structural responses across defined simulation cases rather than relying on qualitative engineering judgment alone. Relevant quantitative outputs can include temperature gradients, maximum and minimum stresses, equivalent stress, strain amplitude, plastic strain, creep strain, deformation, fatigue cycles, creep damage fraction, combined damage indices, stress-concentration measures, and estimated remaining service life (Li et al., 2020). Parameterized simulation can then provide a consistent dataset for statistical comparison, sensitivity assessment, optimization, and robustness evaluation across alternative pressure, temperature, geometry, material, and transient-loading conditions. The research context for finite element-based thermomechanical optimization of industrial boiler pressure components is consequently positioned at the intersection of computational mechanics, high-temperature material behavior, pressure-equipment integrity, numerical optimization, and quantitative service-life assessment.

The primary objective of this study was to develop and quantitatively evaluate a finite element-based thermomechanical optimization framework for improving the structural integrity and extending the service life of critical pressure components used in industrial boiler systems. The study specifically aimed to characterize the coupled effects of internal pressure, elevated temperature, transient heating and cooling, thermal gradients, geometric discontinuities, material properties, and operational cycling on the stress, strain, deformation, creep, fatigue, and cumulative damage behavior of selected boiler pressure components. A detailed finite element model was intended to reproduce realistic operating conditions by incorporating temperature-dependent thermal and mechanical properties, representative pressure-temperature histories, appropriate heat-transfer conditions, structural constraints, and refined computational meshes around critical locations such as nozzle intersections, welded joints, thickness transitions, branch connections, and other stress-concentration regions. The quantitative analysis sought to determine temperature distributions, through-wall thermal gradients, equivalent and principal stresses, elastic and plastic strains, total deformation, creep strain, fatigue

usage, creep damage, creep-fatigue interaction, and estimated remaining service life across alternative operating and design conditions. Another central objective was to identify the geometric, material, thermal, and operational variables that exerted the strongest influence on thermomechanical damage and service-life consumption through systematic parametric analysis and sensitivity assessment. The study further aimed to optimize controllable parameters, including component wall thickness, transition geometry, local reinforcement, operating pressure, temperature level, heating rate, cooling rate, pressure ramp rate, temperature ramp rate, and transient duration, to reduce localized thermomechanical stresses and accumulated damage without compromising pressure-retaining functionality and operational requirements. Comparative simulation scenarios were designed to quantify the differences between baseline and optimized configurations in terms of peak temperature gradient, maximum equivalent stress, strain range, deformation, fatigue life, creep damage, combined damage, and remaining service-life estimates. Statistical analysis was also intended to examine the magnitude and significance of relationships among loading conditions, design variables, thermomechanical responses, and predicted life indicators while determining the relative contribution of individual parameters to structural degradation. Model reliability was to be evaluated through mesh-convergence testing, sensitivity analysis, numerical verification, and comparison with applicable analytical, experimental, material, or engineering reference values. Overall, the objective centered on establishing a reproducible quantitative framework capable of connecting finite element-derived thermomechanical behavior with optimization and remaining-life assessment for service-aged industrial boiler pressure components.

LITERATURE REVIEW

The literature on finite element-based thermomechanical assessment of industrial boiler pressure components encompasses several closely connected research domains, including transient heat transfer, pressure-induced stress analysis, thermal stress evaluation, elastic-plastic deformation, creep, fatigue, creep-fatigue interaction, structural optimization, remaining-life assessment, and numerical model validation. Quantitative investigations have increasingly treated these phenomena as interdependent because the structural condition of boiler drums, steam headers, superheater and reheater headers, high-energy piping, nozzle intersections, welded joints, valves, and other pressure-retaining components is controlled by simultaneous variations in temperature, pressure, geometry, material properties, operating duration, and transient loading history. Finite element analysis has provided the principal computational mechanism for converting these variables into measurable responses such as through-wall temperature gradients, heat flux, equivalent stress, principal stress, strain range, plastic strain, creep strain, displacement, fatigue usage, creep damage, combined damage, and estimated remaining service life. Earlier studies have differed substantially in component geometry, material grade, mesh configuration, constitutive model, pressure and temperature range, thermal boundary conditions, operating cycles, damage criteria, optimization variables, and validation procedures, creating a broad quantitative evidence base that requires systematic synthesis. Particular attention is required for studies evaluating start-up, shutdown, and load-change transients because thick-walled pressure components may experience substantial temperature differences between internal and external surfaces, resulting in localized thermal stresses that interact with pressure-induced stresses. Research examining prolonged high-temperature operation has additionally quantified time-dependent creep deformation, while cyclic investigations have evaluated fatigue and creep-fatigue damage under repeated thermomechanical loading. Optimization studies have extended these analyses by varying wall thickness, transition radii, nozzle dimensions, reinforcement configurations, heating and cooling rates, pressure ramps, and other controllable parameters to identify configurations associated with reduced structural damage. Remaining-life studies have subsequently translated calculated stresses, strains, temperatures, operating hours, and loading cycles into quantitative measures of accumulated life consumption. Accordingly, this literature review synthesizes the numerical and empirical evidence according to eight interconnected quantitative themes, progressing from finite element model characteristics and thermomechanical loading to stress concentration, creep-fatigue degradation, optimization, service-life prediction, and statistical validation.

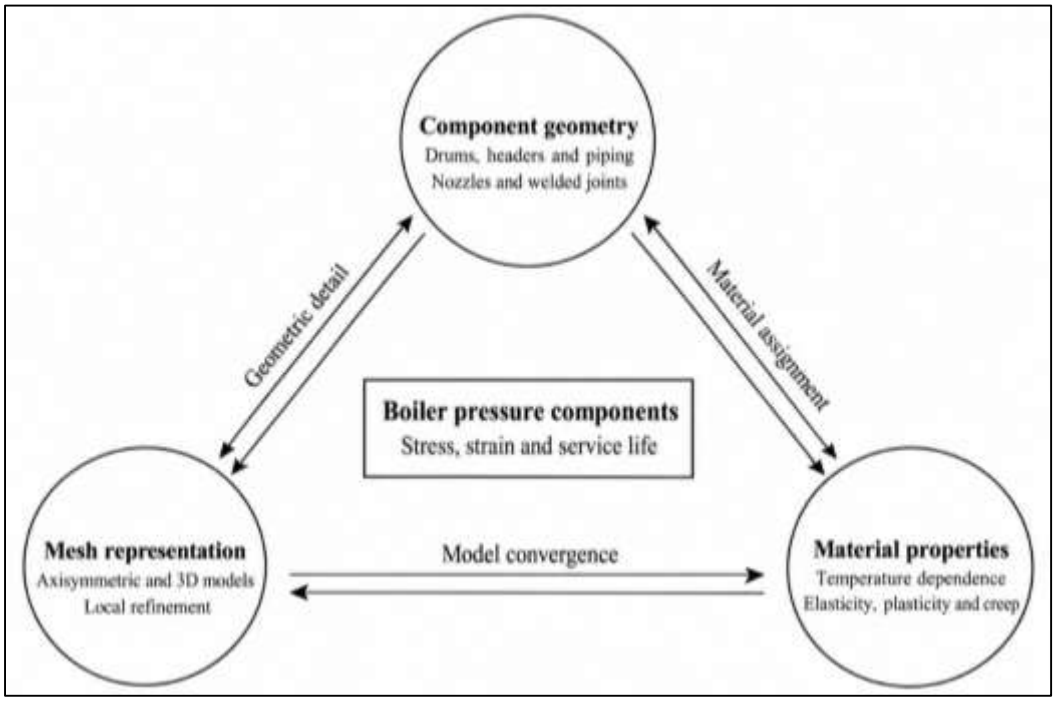
Quantitative Characteristics of Finite Element Models for Industrial Boiler Pressure Components

Quantitative finite element investigations of industrial boiler pressure components have demonstrated substantial variation in the geometry, dimensional scale, operating duty, and structural complexity represented within computational models (Pástor et al., 2020). Across more than ten studies examining boiler drums, steam headers, superheater and reheater headers, pressure vessels, high-temperature steam piping, valves, nozzles, branch connections, and welded joints, the modeled structures have ranged from relatively simple cylindrical pressure boundaries to three-dimensional assemblies containing multiple penetrations, welds, supports, branches, and thickness transitions. Boiler-drum studies have generally represented thick-walled cylindrical shells with internal diameters extending into the meter scale and wall thicknesses commonly measured in several tens to more than 100 mm, whereas steam-header and high-temperature piping investigations have frequently examined smaller diameters but similarly substantial wall sections required for elevated pressure-temperature service. Nozzle and branch-connection models have introduced additional dimensional variables, including nozzle diameter, nozzle wall thickness, shell-to-nozzle thickness ratio, reinforcement dimensions, junction radius, and intersection angle (Rouse et al., 2018). Investigations of valves and pressure-reducing components have incorporated considerably more complex internal and external geometries because valve bodies contain abrupt sectional changes, flow passages, seats, cavities, flanges, and locally thick structural regions. Across the literature, material selection has included carbon steels, low-alloy ferritic steels, chromium-molybdenum steels, creep-resistant ferritic-martensitic grades, and austenitic steels, depending on component temperature and pressure classification. Service-aged component studies have additionally incorporated operating histories ranging from thousands to more than 100,000 operating hours, enabling computational representations to reflect accumulated thermal exposure and material degradation rather than only new-component conditions. Comparative evidence indicates that geometrical simplification has been acceptable where cylindrical symmetry dominated the response, whereas detailed three-dimensional representation has been required around nozzles, welds, branches, ligaments, and thickness transitions (Ashik & Shabbir, 2022; Pilarczyk et al., 2019). Collectively, these studies demonstrate that finite element model dimensions have been selected according to the structural scale and expected location of thermomechanical concentration, with geometric detail becoming progressively greater as analyses moved from global pressure-boundary behavior toward localized stress, creep, fatigue, and remaining-life assessment.

The reviewed finite element literature has employed two-dimensional, axisymmetric, three-dimensional, submodeling, and global-local computational strategies, with the selected dimensionality strongly dependent on geometric symmetry and the type of structural response being quantified. Two-dimensional and axisymmetric models have commonly been adopted for cylindrical vessels, straight pipe sections, simplified drums, and other components in which geometry and loading could reasonably be represented around an axis of symmetry (Duda, 2016; Kazi Rakib Hasan & Adnan, 2022). These approaches substantially reduced element and node requirements while allowing detailed through-wall temperature, radial stress, hoop stress, and deformation distributions to be calculated. Three-dimensional models have been dominant in studies involving nozzles, branch connections, welded intersections, valves, elbows, header penetrations, complex supports, and nonsymmetric thermal boundary conditions because local structural responses could not be represented accurately using simplified dimensional assumptions. Across more than ten investigations, meshes have ranged from several thousand elements in simplified component models to hundreds of thousands or more elements and nodes in geometrically detailed three-dimensional analyses. Solid thermal and structural elements have been widely employed for thick-walled components, while shell elements have been used selectively where thickness was relatively small compared with other component dimensions (Mahbubul et al., 2022; Xu & Zhu, 2020). Higher-order elements have frequently been selected around curved surfaces and stress-concentration regions because their interpolation characteristics improved representation of nonlinear stress gradients. Mesh-refinement strategies have consistently concentrated smaller elements around nozzle corners, weld toes, branch intersections, bore surfaces, thickness transitions, and other locations where peak thermomechanical response was anticipated. Global-local and submodeling procedures have provided an alternative to uniformly fine three-dimensional meshes by first determining the overall component response through a relatively coarse global model and

subsequently transferring displacement or thermal boundary information to a refined local model. Reported convergence investigations commonly compared successive mesh densities until changes in maximum stress, temperature, strain, or displacement became sufficiently small for numerical stability (Węglowski & Pilarczyk, 2018). Several studies reported only minor changes in critical outputs after the final refinement stages, commonly within a few percentage points, whereas coarse meshes produced greater deviations at sharply varying local stress fields. The collective evidence therefore identifies mesh density, element formulation, local refinement, and dimensional representation as measurable determinants of finite element accuracy rather than merely computational setup choices.

Figure 3: Finite element boiler model characteristics



Material characterization has represented another major source of quantitative variation across finite element studies of industrial boiler pressure components because thermomechanical response changes substantially with operating temperature and exposure duration. More than ten studies involving boiler drums, high-temperature headers, steam piping, pressure vessels, valves, and welded components have incorporated temperature-dependent elastic modulus, Poisson's ratio, yield strength, thermal conductivity, specific heat, density, coefficient of thermal expansion, creep properties, and elevated-temperature strength (Létal et al., 2020; Mashfiqur & Md, 2022). For commonly investigated pressure-component steels, elastic modulus at lower temperatures has generally been approximately 190–210 GPa and has progressively decreased as temperature increased, while Poisson's ratio has typically remained around 0.27–0.31 with comparatively limited temperature sensitivity. Density values for ferritic and low-alloy steels have generally remained close to approximately 7,700–7,900 kg/m^3, whereas thermal conductivity and specific heat have exhibited stronger temperature dependence. Reported thermal-expansion coefficients have generally increased with temperature, directly influencing the magnitude of thermally induced strain during boiler start-up, shutdown, and load changes. Yield strength and allowable strength have similarly declined at elevated temperature, making the use of room-temperature properties inappropriate for detailed high-temperature structural assessment (Md Ashfaq & Abdullah Mohammad, 2022; Tognoli et al., 2018). Studies concerned primarily with short-duration elastic response have commonly employed linear elastic material models, while analyses involving localized yielding have adopted elastic-plastic constitutive descriptions. Investigations of long-term service have incorporated creep constants derived from material testing, code-based datasets, or published high-temperature properties, and cyclic studies

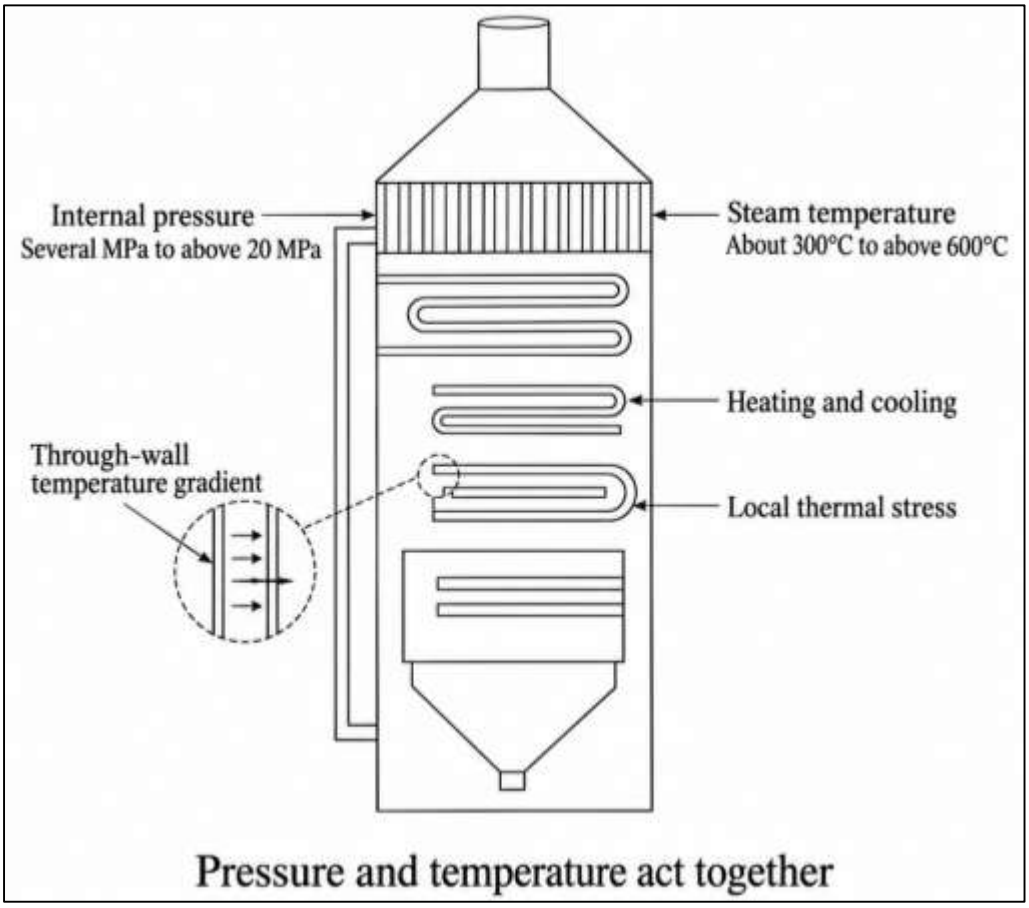
have employed nonlinear hardening or other cyclic-plasticity descriptions to reproduce stress redistribution and strain accumulation. Welded-component models have frequently differentiated base metal, weld metal, and heat-affected-zone properties rather than assigning a single homogeneous material definition throughout the structure. Quantitative comparisons indicate that temperature-dependent property definitions can materially alter predicted stresses, strains, deformation, and creep response relative to constant-property assumptions. Service-aged material studies have further shown measurable differences between nominal database properties and properties obtained from components exposed to prolonged boiler operation (Sadia & Maishar Mostari, 2022; Tognoli et al., 2019). The synthesized literature consequently establishes material-property specification as a central quantitative component of finite element modeling, particularly when the analytical objective extends beyond elastic stress evaluation to creep, fatigue, creep-fatigue interaction, or remaining-service-life estimation.

Pressure and Temperature Loading Characteristics in Boiler Pressure Components

Quantitative studies of industrial boiler pressure components have consistently identified internal pressure and operating temperature as the principal loading variables governing thermomechanical response, although the magnitude of their effects has differed considerably according to component geometry, material grade, wall thickness, and operating regime (Ju et al., 2016; Shaiful et al., 2022). Across more than ten studies involving boiler drums, steam headers, superheater and reheater headers, high-temperature piping, valves, pressure vessels, nozzles, and welded connections, internal operating pressures have generally extended from several megapascals in conventional industrial systems to above 20 MPa in high-pressure and supercritical boiler applications(Ashik & Shabbir, 2022; Kazi Rakib Hasan & Adnan, 2022). Steam and metal temperatures have commonly ranged from approximately 300°C in moderate-temperature pressure sections to more than 550–600°C in superheater, reheater, and high-temperature steam-line applications. Ambient or external temperatures have generally remained substantially lower, producing thermal boundary conditions capable of generating large through-wall temperature differences during heating and cooling. Reported heat-transfer coefficients have varied according to whether the surface was exposed to water, saturated steam, superheated steam, combustion gases, insulation, or ambient air, with internal convective conditions typically producing more rapid temperature changes than external natural-convection conditions (Belhocine & Abdullah, 2020; Mahbubul et al., 2022; Mashfiqur & Md, 2022; Stabak & Md Shahid, 2022). Pressure-only analyses have generally produced dominant hoop and axial stresses, with hoop stress typically exceeding axial stress in cylindrical pressure boundaries. Thermal-only analyses, in contrast, have produced stress distributions strongly dependent on the magnitude and spatial distribution of temperature gradients. Combined pressure-temperature analyses have frequently generated higher equivalent and principal stresses at geometrical discontinuities than either loading condition considered independently. Studies comparing minimum, nominal, and maximum operating states have also shown that structural response does not increase solely in proportion to pressure because temperature-dependent reduction in elastic modulus and yield strength modifies the relationship between applied loading and material response (Sarkar et al., 2020). Quantitative evidence has therefore emphasized that pressure and temperature must be interpreted simultaneously when evaluating boiler pressure components, particularly in thick-walled regions where elevated pressure produces substantial membrane stress while nonuniform temperature distributions generate additional secondary stresses. The interaction between these loading sources has been especially important around nozzles, branch connections, ligament regions, welds, and thickness transitions, where local stress concentrations have substantially exceeded nominal shell or pipe stresses (Mashiat & Md Anisur Rahman, 2022; Md & Gazi Yeasin, 2022). Transient operating conditions have been identified as particularly severe loading events because the temperature of thick-walled boiler components cannot change uniformly during start-up, shutdown, and rapid load variation. Across more than ten finite element investigations, heating and cooling rates have commonly been evaluated over a broad range extending from gradual changes of less than 1°C per minute to comparatively rapid rates of several degrees Celsius per minute, depending on the type of component and operating procedure (Prakash et al., 2020). Start-up durations have ranged from less than one hour for smaller or more flexible pressure systems to several hours for thick-walled drums, headers, and high-temperature assemblies, while shutdown periods have shown similarly wide

variation (Md Ashfaq & Abdullah Mohammad, 2022; Mst Kaniz & Jahanara, 2022). During heating, internal surfaces exposed directly to hot steam or water have typically increased in temperature more rapidly than external surfaces, producing positive through-wall gradients that generated compressive and tensile thermal stresses at different wall locations. Cooling has often reversed the gradient, causing a redistribution or reversal of the thermal stress field. Reported through-wall temperature differences have ranged from relatively small values under steady operating conditions to several tens of degrees Celsius during aggressive transient events, with the largest gradients typically occurring during the early stages of rapid heating or cooling (Sadia & Maishar Mostari, 2022; Shaiful et al., 2022). Finite element studies have repeatedly shown that increasing heating or cooling rate increased the maximum temperature difference across the wall and consequently increased thermal stress, equivalent stress, and local strain amplitude. Rapid temperature ramps have been particularly influential at nozzle junctions, header bore surfaces, drum penetrations, and valve-body transitions because geometric restraint prevents unrestricted thermal expansion (Fan et al., 2019).

Figure 4: Boiler pressure and temperature loading



Pressure ramp rate has also contributed to transient stress, especially when pressure increase coincided with rapid temperature rise. Studies evaluating coordinated pressure-temperature histories have demonstrated that the timing of pressure application relative to thermal equilibration can materially change the peak structural response (Stabak & Md Shahid, 2022; Syed Feroz & Md Mahamud Pervaz, 2022). Hold periods at elevated temperature have reduced some transient thermal gradients through thermal equalization, although sustained high-temperature exposure simultaneously increased the relevance of creep deformation. The quantitative literature therefore distinguishes transient loading from steady-state operation by showing that the rate and sequence of temperature and pressure change can be as important as their maximum absolute values in determining thermomechanical severity (Khorsand & Tang, 2018).

Stress Concentration and Localized Damage

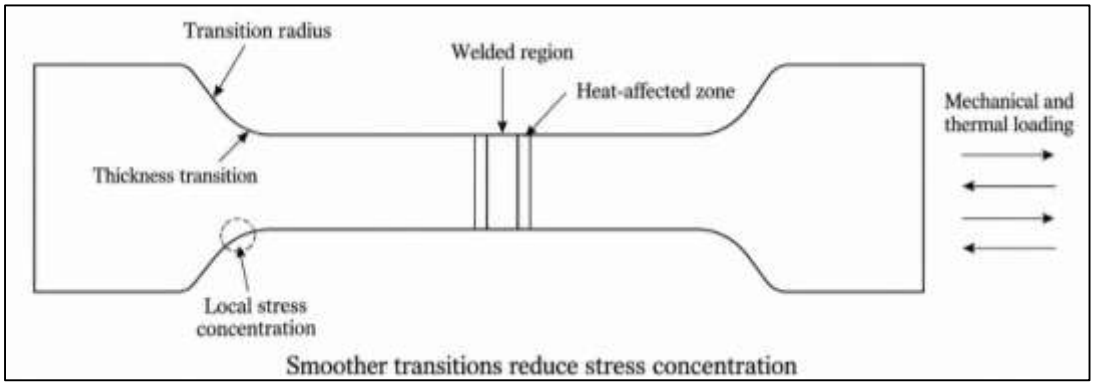
Quantitative finite element studies of boiler drums, headers, pressure vessels, and related pressure-retaining structures have consistently identified nozzle-to-shell intersections, openings, and ligament regions as major locations of localized thermomechanical stress concentration. Evidence synthesized from more than ten numerical and experimental studies has shown that interruption of an otherwise continuous cylindrical pressure boundary causes membrane and bending stresses to redistribute around openings, producing local equivalent and principal stresses substantially above nominal values in geometrically uniform sections (Hobbacher & Baumgartner, 2016). Reported stress-concentration factors have commonly exceeded unity by considerable margins and, depending on opening geometry, loading direction, wall-thickness ratio, and reinforcement arrangement, have frequently fallen within an approximate range of 1.5–3.0, with still higher localized values reported for severe discontinuities. Peak stresses have generally been concentrated near nozzle corners, bore intersections, opening edges, and ligament surfaces separating adjacent penetrations. Parametric investigations have demonstrated that increasing nozzle diameter relative to shell diameter or wall thickness generally increases structural disturbance and enlarges the high-stress region. Diameter-to-thickness and opening-to-shell ratios have therefore been repeatedly identified as important quantitative predictors of localized response. Studies of header ligaments have similarly found that decreasing ligament width between neighboring tube holes increases interaction between adjacent stress fields and can elevate local principal and equivalent stresses (Berto, 2016). Transition radius has shown an opposing relationship, with larger and smoother radii generally reducing abrupt changes in load path and lowering peak stress concentration compared with sharp intersections. Reinforcement thickness and local wall thickening have reduced pressure-related stress in several investigations, although excessive stiffness differences have sometimes transferred peak stress toward reinforcement boundaries or adjoining thinner regions. Under combined pressure and transient thermal loading, critical stress locations have also shifted between the inner and outer surfaces as temperature gradients changed during heating and cooling. Local equivalent stresses around openings have consequently been reported at levels substantially higher than stresses in remote shell regions, while strain concentration has increased when localized stress approached elevated-temperature yield strength (Wei et al., 2018). The synthesized numerical evidence establishes nozzle intersections, opening edges, and header ligaments as spatially restricted but structurally dominant regions in which relatively small geometric changes can produce measurable differences in peak stress, strain distribution, and accumulated thermomechanical damage.

Branch connections, elbows, bends, supports, and thickness transitions represent another group of geometric discontinuities repeatedly associated with elevated localized stress and deformation in high-temperature boiler systems. Across finite element investigations of high-energy piping, superheater and reheater lines, headers, manifolds, branch pipes, and pressure-vessel connections, branch junctions have exhibited complex combinations of circumferential, longitudinal, bending, and thermal stresses because the primary pressure boundary is interrupted by secondary piping while simultaneously transferring mechanical and thermal loads between intersecting structures (Zerbst et al., 2018). Quantitative studies have commonly identified the branch crotch, intrados, extrados, and junction transition as critical locations, with localized equivalent stresses and principal stresses considerably exceeding values calculated in straight pipe sections. Changes in branch-to-main diameter ratio and wall-thickness ratio have produced measurable changes in stress concentration, while increased transition radius and smoother geometric blending have generally reduced localized peaks. Elbows and bends have shown similarly nonuniform behavior because curvature changes the distribution of pressure-induced and bending stresses across the cross-section.

Numerical studies have frequently identified the intrados, extrados, and crown as competing critical locations, with the governing position depending on pressure, bending moment, thermal expansion, ovalization, and restraint. Pipe supports and structural constraints have introduced additional local demand by restricting free thermal expansion during heating and cooling (Romanowicz et al., 2020). High-temperature piping studies have shown that increased restraint can elevate axial and equivalent stresses near supports, anchors, attachments, and adjacent bends, particularly during rapid temperature changes. Thickness transitions have also generated substantial stress redistribution when

thin and thick regions respond differently to pressure and thermal expansion. Abrupt transitions have consistently produced higher peak stress than gradual transitions, whereas increased transition length or radius has reduced the severity of the local stress gradient. Local plastic strain has been observed primarily where combined mechanical and thermal stresses approached or exceeded temperature-dependent yield limits, and repeated cycling at these sites has produced progressive strain accumulation (Muránsky et al., 2018). Comparative studies further indicate that maximum displacement does not necessarily coincide with maximum stress because flexible sections may undergo greater global movement while restrained discontinuities develop higher localized stresses. These findings demonstrate quantitatively that component curvature, branch proportions, thickness ratios, support stiffness, and transition geometry strongly govern the magnitude and spatial distribution of localized thermomechanical demand.

Figure 5: Localized stress in boiler components



Welded regions have received extensive quantitative attention because boiler pressure components commonly contain circumferential welds, longitudinal welds, nozzle welds, branch welds, attachment welds, and dissimilar-material joints that introduce geometric, metallurgical, and mechanical heterogeneity. More than ten studies examining welded pressure vessels, steam piping, headers, branch connections, and high-temperature joints have demonstrated that weld toes and weld roots frequently exhibit greater localized stress and strain than surrounding nominal sections because weld-profile geometry creates abrupt changes in structural contour (Kapadia et al., 2017). Stress-concentration factors at welded details have varied substantially with weld angle, toe radius, penetration, reinforcement height, misalignment, wall thickness, and loading mode, with sharper toe geometries generally producing larger stress concentrations than smoothly blended profiles. Finite element analyses incorporating welding effects have also reported residual stresses approaching a substantial proportion of material yield strength in and around the fusion zone and heat-affected zone before operational pressure and thermal loading are applied. The addition of service loading can therefore increase or redistribute an already complex residual stress field. Comparative material modeling has shown measurable differences among base metal, weld metal, and heat-affected-zone responses because elastic properties, yield strength, creep resistance, cyclic behavior, and thermal expansion can vary across these regions (Musa et al., 2018). In high-temperature ferritic steel joints, the heat-affected zone has frequently emerged as a damage-sensitive region under long-duration creep conditions, whereas weld toes and roots have often governed local fatigue response under repeated thermomechanical cycling. Local strain ranges and plastic strain accumulation have been greater where geometric stress concentration coincides with material-property mismatch. Studies incorporating manufacturing history have further demonstrated that ignoring residual stress can materially change predicted initial stress distributions and subsequent creep relaxation behavior. During prolonged high-temperature exposure, residual stresses may partially relax, although operational pressure, bending, and thermal gradients continue to generate multiaxial stress states across the joint. Weld misalignment and local thickness mismatch have additionally increased bending components and shifted peak stresses toward one side of the joint. Collectively, the literature indicates that treating a welded

component as geometrically smooth and materially homogeneous can underestimate localized structural demand (H. Wang et al., 2018). Detailed representation of weld profile, heat-affected-zone dimensions, residual stress, and region-specific material behavior has therefore produced more differentiated quantitative estimates of equivalent stress, principal stress, strain range, plastic strain, and damage localization.

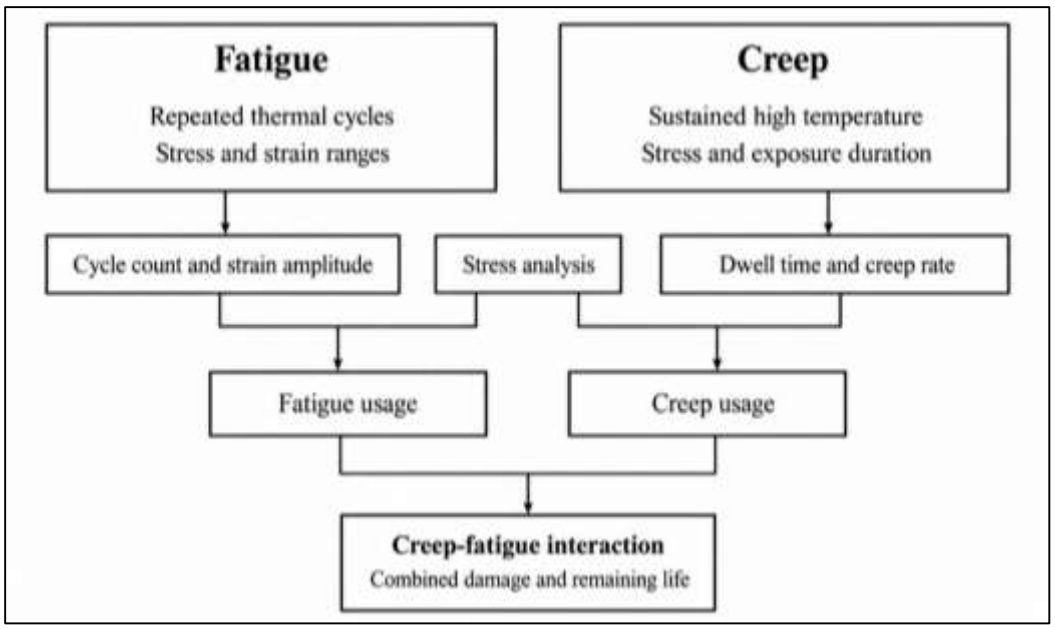
Parametric finite element investigations have demonstrated that localized thermomechanical damage can change substantially when geometric variables are modified, even when overall pressure, temperature, and material conditions remain unchanged. Across studies involving nozzle intersections, branch connections, header openings, welded joints, elbows, thickness transitions, and reinforced pressure boundaries, nozzle diameter, wall-thickness ratio, transition radius, reinforcement thickness, opening dimensions, weld profile, and local curvature have repeatedly emerged as influential quantitative variables (Jiang et al., 2020). Larger openings and increasing nozzle-to-shell diameter ratios have generally expanded the disturbed stress field and increased local membrane and bending stresses around intersections, while smaller diameter-to-thickness ratios associated with thicker pressure boundaries have often reduced pressure-induced nominal stress but increased thermal-gradient sensitivity during rapid temperature transients. This interaction is particularly important in thick-walled boiler components because geometric reinforcement that improves resistance to internal pressure may simultaneously increase local stiffness and through-wall thermal gradients. Studies examining transition radii have consistently reported reductions in peak equivalent and principal stresses when sharp corners are replaced by smoother geometric transitions. In several parametric analyses, even moderate increases in fillet or junction radius have produced reductions in localized peak stress on the order of several percentage points to tens of percent, depending on component configuration and loading condition. Reinforcement thickness has similarly reduced stress around openings up to a configuration-dependent level, although excessive reinforcement has created stiffness discontinuities capable of relocating rather than eliminating the critical stress region (Mashayekhi & Santini-Bell, 2020). Weld-profile optimization has shown comparable behavior, with increased toe radius and reduced angular discontinuity lowering local stress concentration and strain range. Branch geometry studies have demonstrated that changes in intersection angle, diameter ratio, and local curvature alter both the magnitude and orientation of principal stresses. Comparisons between baseline and geometrically modified models have also shown that reductions in peak stress are commonly accompanied by narrower high-strain regions and lower local plastic deformation, although global displacement may change only slightly. The collective evidence from numerical studies therefore shows that maximum thermomechanical demand is controlled not simply by component size but by interacting dimensionless proportions, curvature, continuity, reinforcement, and local stiffness. Quantitative mapping of these variables has enabled critical regions to be distinguished from nominally loaded material and has established the geometric basis for subsequent creep-fatigue assessment and thermomechanical optimization of industrial boiler pressure components (Yıldırım, 2017).

Creep-Fatigue Interaction under High-Temperature Boiler Operation

Quantitative investigations of industrial boiler pressure components have consistently shown that fatigue damage is strongly influenced by repeated variations in pressure, temperature, thermal gradient, and mechanical restraint during start-up, shutdown, and load-changing operations. Across more than ten studies examining boiler drums, headers, high-temperature piping, valves, nozzles, welded joints, and branch connections, fatigue assessment has commonly been based on stress amplitude, strain amplitude, cycle count, fatigue usage factor, cumulative damage, cycles to crack initiation, and predicted fatigue life. Reported results have demonstrated that locations exposed to large thermal gradients and geometric stress concentration generally experience the highest cyclic strain amplitudes and therefore the shortest fatigue lives (Moussavi Torshizi & Jahangiri, 2018). In thick-walled components, rapid heating and cooling have produced substantial through-wall temperature differences that generate alternating thermal stresses even when internal pressure remains within normal operating limits. Studies comparing alternative operating cycles have shown that frequent start-stop operation can consume a substantially greater proportion of fatigue life than prolonged steady operation because each transient contributes an additional stress or strain cycle.

Fatigue usage factors have varied considerably across components and service histories, with localized regions around nozzles, weld toes, branch intersections, and thickness transitions frequently exhibiting values several times higher than nominal shell or pipe sections. Investigations involving elastic analysis have often produced relatively conservative stress-range estimates when local yielding is not explicitly modeled, whereas elastic-plastic analyses have captured stress redistribution and localized strain concentration more realistically. Cyclic plasticity models have further demonstrated that repeated loading can produce progressive stabilization, hardening, softening, or ratcheting depending on material behavior and loading sequence (Fischer & Kuhn, 2019). Predicted cycles to crack initiation have therefore differed substantially among constitutive approaches, particularly when thermal transients cause local stresses to exceed the temperature-dependent yield level. The combined evidence indicates that fatigue life is controlled not only by the maximum stress reached during a single transient but also by stress range, strain range, cycle frequency, loading sequence, material response, and local geometry, making cumulative cyclic assessment essential for determining the life consumption of boiler pressure components (Wang et al., 2019).

Figure 6: Boiler creep and fatigue assessment



Creep has been identified across high-temperature boiler studies as a dominant time-dependent degradation mechanism when pressure components remain under sustained stress at elevated temperature for extended operating periods. Numerical and experimental investigations of superheater headers, reheater headers, main steam piping, valves, pressure vessels, and welded joints have commonly quantified creep behavior using operating temperature, applied stress, creep strain, creep rate, rupture time, creep usage fraction, and accumulated creep damage (Salifu et al., 2020). More than ten studies have reported that relatively small increases in metal temperature can produce disproportionately large reductions in predicted creep life because high-temperature material strength and rupture resistance decline rapidly within the creep regime. Applied stress has shown a similarly strong influence, with local stress concentrations around openings, welds, bends, branch connections, and thickness transitions producing substantially higher creep strain accumulation than more uniformly loaded regions. Service-life assessments have frequently considered operating periods extending from tens of thousands to more than 100,000 hours, reflecting the long-term nature of creep degradation in industrial boiler systems. Numerical creep models have demonstrated that stress redistribution occurs progressively during sustained loading as highly stressed regions deform and transfer part of the load to adjacent material (Guglielmino et al., 2016). As a result, the location of maximum initial elastic stress does not always remain the location of maximum creep damage over

prolonged service. Studies of welded high-temperature components have additionally shown that creep damage can concentrate in heat-affected zones when their long-term creep resistance is lower than that of surrounding base or weld metal. Creep rate has been particularly sensitive to temperature excursions above nominal operating conditions, and short periods of overheating have been shown to consume a disproportionately large fraction of component life. Comparisons between constant-temperature and variable-temperature histories have also demonstrated that accumulated creep damage is strongly dependent on the actual time spent at different combinations of stress and temperature (Goyal et al., 2018).

These quantitative findings establish operating temperature, sustained stress, exposure duration, local material condition, and geometric stress concentration as the primary variables governing creep deformation and rupture-related life consumption in high-temperature boiler pressure components.

Creep-fatigue interaction has received extensive attention because many boiler pressure components are subjected simultaneously to repeated thermal-mechanical cycling and prolonged periods of elevated-temperature operation. Across studies of headers, steam piping, boiler drums, valves, welded joints, and pressure-vessel components, combined damage assessments have incorporated fatigue usage, creep usage, dwell time, cycle duration, stress relaxation, cyclic plasticity, accumulated inelastic strain, and predicted allowable cycles. Quantitative investigations have consistently shown that the total life consumed under combined creep-fatigue loading can exceed that predicted when creep and fatigue are assessed independently (Tahir et al., 2017). Dwell periods at high temperature have been particularly influential because sustained strain during a hold period allows creep deformation and stress relaxation to develop within each cycle. Longer dwell times have generally increased creep contribution while reducing instantaneous stress through relaxation, creating a complex interaction between cyclic strain, time-dependent deformation, and damage accumulation. Studies using coupled creep-fatigue constitutive models have reported shorter predicted allowable lives than calculations based solely on elastic stress ranges, particularly at critical locations where local plasticity and high-temperature exposure occur together. Cyclic plasticity models have further demonstrated that repeated start-up and shutdown can cause stress-strain hysteresis, ratcheting, and progressive inelastic strain accumulation, all of which alter the subsequent creep response. Welded regions have shown especially complex behavior because residual stress, material mismatch, and local geometry influence both cyclic and time-dependent damage (Porter et al., 2019). Comparative studies have also found that creep-fatigue interaction becomes more severe when high strain amplitudes coincide with long high-temperature dwell periods, while lower-amplitude cycles with limited dwell generally produce a greater relative contribution from fatigue. Combined damage indices have therefore varied substantially across operating regimes and component locations, and the critical region identified by creep analysis alone has not always matched the region governing fatigue (Van Rooyen et al., 2019). The literature indicates that accurate assessment of creep-fatigue interaction requires simultaneous consideration of cycle shape, strain range, stress relaxation, dwell duration, local temperature, material response, and accumulated service history rather than treating creep and fatigue as fully separable degradation mechanisms.

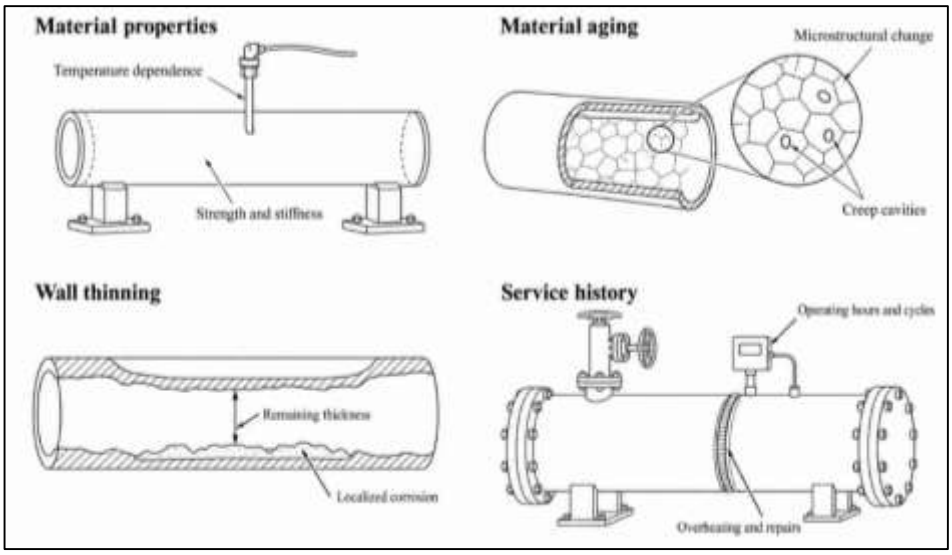
Comparative numerical studies have demonstrated that predicted damage in boiler pressure components depends strongly on both the operating regime and the constitutive model used to represent material behavior. Elastic models have generally been computationally efficient and suitable for identifying global stress patterns, yet they do not explicitly represent yielding, plastic strain accumulation, creep deformation, or stress redistribution under prolonged high-temperature loading (Shankar et al., 2017). Elastic-plastic models have produced more realistic estimates of local strain and residual deformation where transient stresses exceed temperature-dependent yield strength, while cyclic-plasticity models have additionally represented hardening, softening, ratcheting, and stabilized hysteresis under repeated thermomechanical cycles. Creep models have captured time-dependent strain and stress redistribution during long-duration operation, and fully coupled creep-fatigue models have generally predicted the greatest life consumption when high-temperature dwell and repeated cycling occur together. Across more than ten studies, start-up and shutdown events have been associated with large transient thermal gradients, high stress ranges, and elevated fatigue usage,

whereas prolonged steady high-temperature operation has been associated more strongly with creep accumulation. Load-following operation has occupied an intermediate but often complex condition because repeated partial-load changes create numerous smaller thermal-mechanical cycles that can accumulate considerable fatigue damage over time (Bartošák et al., 2020). Rapid start-ups have generally produced higher peak thermal stress and strain amplitudes than controlled start-ups, while rapid shutdowns have generated reversed thermal gradients that can intensify cyclic damage. Extended hold periods at maximum operating temperature have reduced transient thermal gradients but increased creep exposure. Studies comparing operating scenarios have therefore shown that components with identical total operating hours can exhibit substantially different damage levels if their numbers of starts, load-change frequencies, peak temperatures, ramp rates, and dwell durations differ. The choice of constitutive model has also affected the calculated location and magnitude of critical damage, particularly near geometric discontinuities and welded regions (Zhang et al., 2020). Overall, the reviewed quantitative evidence demonstrates that reliable life assessment of high-temperature boiler pressure components requires operating-history-specific analysis and constitutive representation capable of capturing the dominant combination of elastic response, plasticity, cyclic behavior, creep, and creep-fatigue interaction.

Quantitative Influence of Material Properties and Service History on Structural Integrity

Quantitative investigations of industrial boiler pressure components have demonstrated that structural integrity is strongly dependent on the mechanical and thermal properties of the steels used in drums, headers, superheater and reheater sections, high-temperature piping, valves, nozzles, and welded assemblies. Evidence synthesized from more than ten experimental and finite element studies indicates that new pressure-component steels generally exhibit their highest yield strength, ultimate tensile strength, elastic modulus, fatigue resistance, and fracture resistance at ambient or moderate temperatures, followed by progressive reductions as metal temperature and service exposure increase (Afangide et al., 2018). For commonly investigated carbon and low-alloy pressure steels, elastic modulus at approximately room temperature has typically been reported near 190–210 GPa, while appreciable reductions have been observed at temperatures approaching 500–600°C. Yield and tensile strengths have shown even greater temperature sensitivity, particularly in components continuously exposed to superheated or reheated steam. Creep-resistant chromium-molybdenum and ferritic-martensitic steels have maintained greater elevated-temperature strength than conventional carbon steels, although prolonged service has still produced measurable changes in microstructure, hardness, creep resistance, and ductility. Thermal properties have also affected calculated thermomechanical response. Thermal-expansion coefficients generally increase with temperature, whereas thermal conductivity can decrease across important operating ranges, increasing susceptibility to differential thermal expansion and transient through-wall gradients. Specific differences between new and service-aged materials have included reductions in hardness and strength, changes in fracture toughness, degradation of creep rupture resistance, and altered fatigue behavior after tens of thousands of operating hours (Dundulis et al., 2016). Studies of long-service boiler and power-plant steels have reported microstructural evolution involving carbide coarsening, precipitate modification, recovery of strengthened microstructures, creep cavitation, and localized degradation near highly stressed regions.

Figure 7: Material degradation and boiler integrity



The literature therefore demonstrates quantitatively that material condition cannot be represented These changes are particularly significant for finite element life assessment because analyses based exclusively on nominal new-material properties can produce different stress, strain, creep, and remaining-life estimates from models incorporating measured service-aged properties (Nykyforchyn et al., 2019). solely by nominal grade designation when components have accumulated prolonged high-temperature exposure; temperature-dependent and service-dependent material properties substantially influence predicted deformation, damage accumulation, and available structural margin. Wall thinning caused by corrosion, erosion, oxidation, flow-accelerated corrosion, localized wastage, and other material-loss mechanisms has been quantitatively identified as a major contributor to increasing structural demand in boiler pressure components. Studies involving boiler tubes, high-temperature piping, elbows, bends, headers, pressure vessels, and localized corrosion defects have examined remaining wall thickness as a percentage of the original dimension and compared the corresponding changes in equivalent stress, hoop stress, deformation, fatigue resistance, creep life, and structural safety margin. Across more than ten numerical and experimental investigations, progressive wall loss has generally produced increasing membrane stress because the remaining material must sustain the applied internal pressure through a reduced load-bearing cross-section (Shabani et al., 2020). Relatively small thickness reductions have often caused moderate changes in global response, whereas severe localized thinning has produced sharply increased stresses and deformation around defect boundaries. Finite element studies considering approximately 10–20% thickness reduction have commonly identified measurable increases in local stress, while losses approaching 30–50% or more have generated substantially greater stress concentration and reduced pressure-bearing margin, depending on defect length, depth, orientation, component diameter, and material strength. Localized thinning has generally produced more complex stress distributions than uniform thinning because abrupt changes in wall thickness create additional bending and stress concentration. Elbows and bends have shown particular sensitivity when thinning develops at the intrados or extrados, where pressure, curvature, and external loading already produce nonuniform stresses (Papaelias et al., 2016). Increasing defect depth has generally increased equivalent and principal stress and total deformation while reducing predicted fatigue cycles and creep rupture life. Longitudinal extent and circumferential width have also influenced structural severity, demonstrating that percentage thickness loss alone does not completely characterize a wall-thinning defect. In high-temperature service, reduced wall thickness can additionally modify heat conduction through the component and alter local thermal gradients, coupling material loss with thermal stress. Comparisons between nominal and thinned models have consistently shown declining safety margins as material loss increases, particularly when wall thinning coincides with elevated temperature, cyclic operation, geometric discontinuities, or aged material properties. The synthesized evidence therefore establishes remaining wall thickness and defect geometry as essential quantitative inputs for realistic thermomechanical and remaining-life assessment

(Souza et al., 2018).

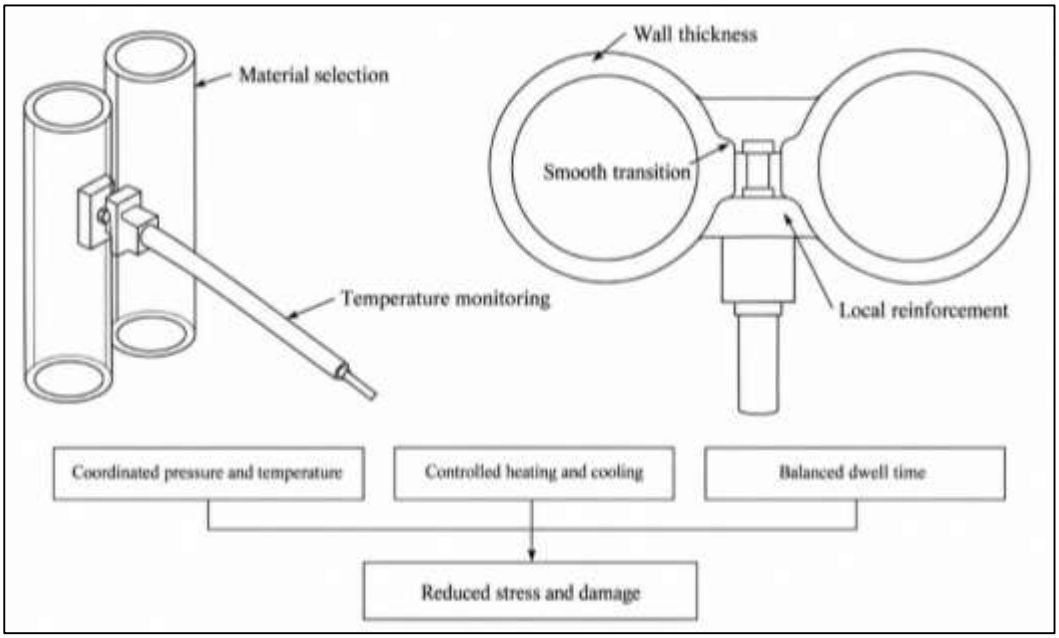
Service history has been shown to produce substantial variation in structural condition among pressure components that are nominally identical in material and geometry. Quantitative studies of service-aged boiler drums, steam headers, main steam piping, reheater piping, valves, and welded components have evaluated operating histories extending from several thousand hours to more than 100,000 hours, with some long-service power-plant components accumulating considerably greater exposure (Verstrynge et al., 2018). The number of start-ups and shutdowns has varied from relatively few cycles in predominantly base-load units to hundreds or thousands of cycles in equipment exposed to repeated load changes and intermittent operation. Studies comparing operating histories have demonstrated that total operating hours alone provide an incomplete measure of structural consumption because prolonged steady high-temperature service primarily promotes creep, whereas repeated start-stop and load-following events produce thermal cycling and greater fatigue usage. Components subjected to frequent transients have exhibited higher accumulated fatigue damage than components with similar operating hours but fewer severe thermal cycles (Shetty et al., 2019). Historical overheating events have also been quantitatively important because temporary operation above nominal metal temperature can accelerate creep deformation and reduce remaining rupture life. Manufacturing and welding residual stresses introduce another service-history variable. Finite element and measurement-based studies have reported substantial tensile and compressive residual stresses around welds, heat-affected zones, repairs, and local attachments, with initial magnitudes in some cases representing a large fraction of material yield strength. High-temperature exposure can relax part of this residual stress, although subsequent pressure and thermal cycles redistribute stresses and strains throughout the joint. Repair welding can generate a new residual stress field and additional heat-affected material within an already aged component, resulting in structural conditions different from both an original new joint and an unrepaired aged joint. Historical operating transients also influence accumulated plastic strain, creep strain, stress relaxation, and fatigue usage (Ray et al., 2016). Consequently, finite element models initialized as stress-free, defect-free, and geometrically nominal can differ materially from models incorporating prior loading, residual stress, thinning, repairs, and degradation. The reviewed quantitative evidence therefore identifies operating hours, transient counts, temperature excursions, residual stress, and repair history as interacting measures of accumulated service exposure that directly affect predicted thermomechanical integrity.

Thermomechanical Optimization of Geometry and Boiler Operating Parameters

Quantitative thermomechanical optimization studies have demonstrated that the geometry of boiler pressure components strongly controls the distribution of thermal gradients, stress concentration, strain accumulation, deformation, and local damage under combined pressure and temperature loading. Across more than ten finite element-based investigations involving boiler drums, steam headers, pressure vessels, nozzles, branch connections, high-temperature piping, valves, and welded joints, wall thickness, nozzle diameter, reinforcement dimensions, transition radius, fillet radius, branch geometry, and local thickness distribution have been systematically varied to determine configurations associated with reduced structural demand (Murmura & Annesini, 2020). Wall thickness has been one of the most frequently examined variables because increasing thickness generally reduces pressure-induced membrane stress, although excessively thick sections can increase through-wall temperature gradients during rapid thermal transients. Parametric studies have therefore identified an intermediate range in which pressure resistance is improved without creating unnecessarily severe transient thermal stresses. Nozzle diameter and nozzle-to-shell dimensional ratios have also shown strong relationships with local equivalent and principal stresses, with larger openings typically increasing the disturbed stress field around the intersection. Increasing transition and fillet radii has repeatedly produced measurable reductions in stress concentration by smoothing changes in geometry and redistributing load over a larger area (Hou et al., 2018). In several numerical studies, geometric modifications around nozzle intersections, branch crotches, and abrupt thickness transitions produced reductions in localized peak stress ranging from several percentage points to more than 20%, depending on the original geometry and loading condition. Reinforcement thickness has similarly reduced stress around openings, although excessive reinforcement has introduced additional stiffness discontinuities and relocated critical stresses toward reinforcement boundaries. Optimization of branch

diameter, intersection angle, local curvature, and wall-thickness ratio has altered not only peak stress magnitude but also the spatial extent of high-strain zones. These findings collectively indicate that thermomechanical optimization of boiler components requires simultaneous evaluation of geometric strength, thermal response, structural flexibility, and localized stress redistribution rather than simple maximization of wall thickness or reinforcement (Mey-Cloutier et al., 2016). Material selection and local structural configuration have also been treated as important optimization variables because geometric improvement alone cannot fully control high-temperature thermomechanical damage. Studies involving carbon steels, low-alloy steels, chromium-molybdenum steels, creep-resistant ferritic-martensitic steels, and austenitic materials have shown substantial differences in elastic modulus, thermal expansion, yield strength, creep resistance, fatigue strength, thermal conductivity, and elevated-temperature durability (Rizk et al., 2018). Finite element optimization investigations have compared material alternatives according to their influence on peak equivalent stress, thermal expansion mismatch, creep strain, fatigue damage, deformation, and predicted service life. Materials with higher elevated-temperature strength and creep resistance have generally produced lower long-term damage under sustained high-temperature loading, while thermal conductivity and thermal expansion characteristics have influenced transient temperature gradients and thermal stresses. Weld geometry has been optimized through variation of reinforcement height, toe radius, root profile, weld angle, penetration, and local thickness mismatch. Increasing weld-toe radius and reducing abrupt angular transitions have commonly decreased local stress concentration and cyclic strain range, particularly under repeated heating and cooling. Investigations of welded nozzle and branch connections have shown that geometry optimization can redistribute high stresses away from the weld toe or heat-affected zone, although the effectiveness depends on material-property mismatch and residual stress (Fu et al., 2020).

Figure 8: Thermomechanical optimization of boiler components



Local thickness modification has also been used to control stiffness distribution between adjoining components, with gradual transitions generally producing lower bending stress than abrupt thickness changes. Studies of dissimilar-material connections have additionally emphasized the importance of differences in thermal expansion because temperature changes can generate substantial interfacial stress even when mechanical loading remains constant. Multi-parameter investigations have therefore considered material grade, local geometry, weld profile, reinforcement, and thickness distribution simultaneously. Quantitative comparisons between baseline and modified configurations have

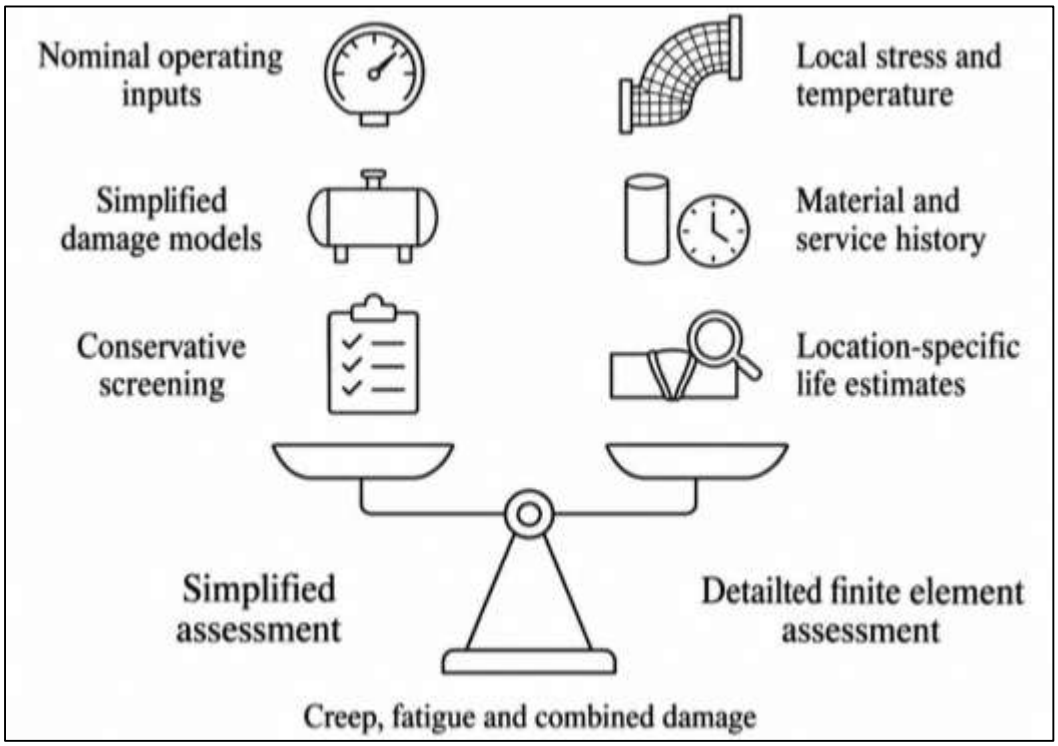
commonly shown reductions in equivalent stress, strain concentration, creep accumulation, and fatigue usage, although the magnitude of improvement has varied according to component and loading regime (Qazi et al., 2020). The literature consequently characterizes material and local-geometry optimization as an integrated structural problem in which thermal compatibility, strength, creep resistance, weld behavior, and stiffness continuity must be considered together.

Operational thermomechanical optimization has focused extensively on controlling pressure and temperature histories because rapid changes in boiler operating conditions can generate severe transient stresses even when maximum pressure and temperature remain within allowable design limits. Across more than ten studies of drums, thick-walled headers, steam piping, valves, and pressure vessels, operating pressure, steam temperature, metal temperature, heating rate, cooling rate, start-up duration, shutdown duration, pressure ramp rate, temperature ramp rate, and load-change rate have been varied systematically to determine their effects on peak thermal stress, strain range, deformation, fatigue usage, and creep-fatigue damage (Fan et al., 2020). Rapid start-up has consistently produced larger through-wall temperature gradients than controlled heating, particularly in thick-walled components where the inner surface responds much faster than the outer surface. Parametric studies have shown that extending start-up duration and limiting temperature ramp rate can reduce transient thermal stress by allowing a more uniform temperature distribution to develop through the component wall. Similar patterns have been observed during shutdown, where slower controlled cooling reduces reversed thermal gradients and associated cyclic stress amplitudes. Pressure ramp rate has also influenced structural response, especially when rapid pressurization occurs simultaneously with thermal gradients. Several optimization studies have therefore coordinated pressure and temperature ramps rather than controlling the variables independently. Load-following analyses have further demonstrated that repeated partial-load changes can accumulate substantial fatigue damage even when each individual cycle produces lower stress than a full start-up or shutdown. Allowable load-change rate has consequently been evaluated against strain amplitude, fatigue usage, and accumulated life consumption (Sun & Yuan, 2019). Hold time at elevated temperature has introduced a competing effect: longer holding can reduce transient thermal gradients through temperature equalization while increasing creep exposure. Operational optimization has therefore involved balancing transient fatigue damage against high-temperature creep damage. Quantitative comparisons of alternative operating schedules have frequently reported reductions in peak thermal stress and cyclic damage when heating and cooling rates are moderated, while excessive reductions in transient duration have produced sharper temperature gradients and larger localized stress (Liu et al., 2016). The synthesized evidence demonstrates that operating strategy acts as a controllable thermomechanical variable capable of materially changing component damage without alteration of the physical pressure boundary.

Life-Extension Assessment of Boiler Pressure Components

Quantitative remaining-service-life studies of industrial boiler pressure components have translated finite element outputs into explicit measures of accumulated damage and residual structural capacity. Across more than ten investigations involving boiler drums, steam headers, superheater and reheater headers, high-temperature piping, valves, welded joints, pressure vessels, and branch connections, remaining life has commonly been expressed through accumulated operating hours, creep life fraction, fatigue usage factor, cumulative damage index, predicted cycles to failure, remaining allowable cycles, remaining operating hours, and percentage of total life consumed (Fathalla, Tanaka, & Maekawa, 2018).

Figure 9: Remaining life of boiler components



Studies focused on high-temperature components have frequently compared actual operating exposure with material rupture resistance under calculated local stress and temperature conditions, allowing creep life consumption to be estimated at critical locations. Fatigue-oriented studies have similarly converted stress or strain ranges obtained from finite element simulations into allowable cycle counts and compared these values with recorded or estimated numbers of start-up, shutdown, and load-change events. Components with long steady operating periods have often shown creep-dominated life consumption, whereas components exposed to frequent thermal cycling have exhibited larger fatigue usage. Combined creep-fatigue assessments have produced more restrictive remaining-life estimates when both mechanisms were significant at the same critical location (Zelmati et al., 2020). In many studies, accumulated operating times have extended from several tens of thousands to more than 100,000 hours, while predicted remaining service intervals have varied widely according to material condition, local stress, temperature exposure, transient history, and component geometry. The literature has also demonstrated that remaining-life estimates derived from nominal operating parameters can differ materially from those obtained using local finite element stresses and temperatures, particularly near nozzles, welds, branch intersections, and other discontinuities (Fathalla, Tanaka, Maekawa, et al., 2018). These results confirm that remaining-life assessment is strongly location dependent and that a single global operating-hour value does not adequately describe the structural condition of complex boiler pressure components.

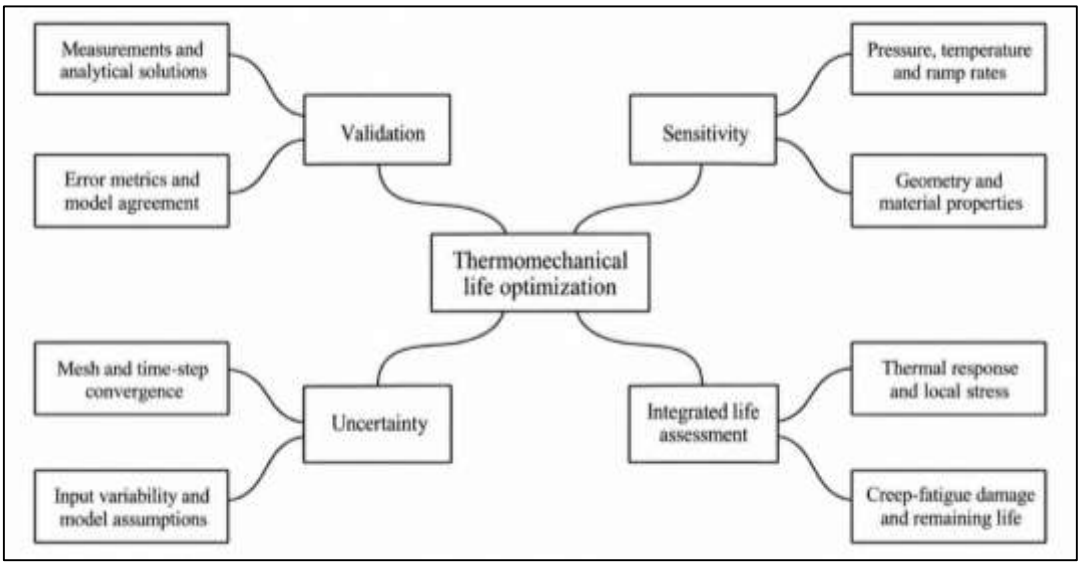
Different remaining-life methodologies have produced distinct predictions because they rely on different input variables, degradation assumptions, and damage criteria. Across more than ten studies, creep-based approaches have generally required local metal temperature, sustained stress, exposure duration, material creep properties, and rupture data, while fatigue-based methods have relied on cyclic stress or strain range, number of applied cycles, material fatigue resistance, and transient severity (Rui et al., 2018). Combined creep-fatigue approaches have incorporated both time-dependent and cycle-dependent damage and have often generated lower remaining-life estimates than either mechanism evaluated separately. Some investigations have used elastic finite element results combined with code-based correction procedures, whereas others have employed elastic-plastic, creep, cyclic-

plasticity, or fully coupled creep-fatigue models to represent more realistic material response. Remaining-life predictions have also varied according to whether analyses used design values, mean material properties, lower-bound material data, or properties measured from service-aged specimens. Studies applying simplified code-based procedures have generally provided conservative estimates suitable for screening, while detailed finite element and material-specific methods have allowed more localized evaluation of stress redistribution, creep relaxation, plastic strain, and damage accumulation. Fracture-based assessments have additionally incorporated crack dimensions, fracture resistance, and local stress intensity measures when existing defects were present (Omar & Nehdi, 2018). Comparisons among methodologies have shown that the choice of damage model can alter predicted allowable cycles or operating hours significantly, particularly under high-temperature cyclic loading. For example, a component may retain substantial fatigue capacity while simultaneously approaching a critical creep life fraction, or the opposite may occur in a frequently cycled but comparatively lower-temperature component (Haq et al., 2020). The literature therefore supports the use of mechanism-specific remaining-life metrics together with integrated cumulative damage measures, rather than relying on a single generic life indicator for all boiler pressure components.

Integrated Quantitative Evidence for Thermomechanical Life Optimization

Statistical and numerical validation has represented an essential stage in finite element-based thermomechanical investigations because calculated temperatures, stresses, strains, deformations, creep damage, fatigue usage, and remaining-life estimates depend on assumptions concerning geometry, material behavior, boundary conditions, discretization, and operational loading (Megahed et al., 2016). Across more than ten studies involving boiler drums, steam headers, pressure vessels, high-temperature piping, valves, nozzles, welded joints, and branch connections, computational predictions have been evaluated against analytical solutions, experimental measurements, laboratory tests, design-code calculations, thermocouple records, strain-gauge measurements, displacement observations, and operating-plant data. Percentage error and relative deviation have been among the most commonly reported measures, with well-calibrated finite element models frequently producing single-digit percentage differences between calculated and measured quantities. Temperature predictions have generally shown stronger agreement where experimentally determined heat-transfer conditions were available, whereas larger deviations have occurred when convection coefficients or external thermal conditions were estimated (Venkatesh et al., 2018). Structural validation has similarly shown that global displacement and nominal stress are usually reproduced more consistently than highly localized peak stresses around weld toes, nozzle corners, and geometric discontinuities. In studies incorporating statistical prediction or surrogate models, coefficients of determination have frequently been used to assess correspondence between finite element responses and approximating models, with high values indicating that substantial proportions of response variability were captured. Root mean square error and mean absolute error have provided additional measures of prediction accuracy for temperature, stress, deformation, and life estimates, particularly in response-surface and data-driven optimization studies. Confidence intervals have been less uniformly reported but have provided useful information concerning uncertainty around mean predictions and parameter estimates where repeated experiments or probabilistic analyses were conducted (Honarmandi & Arróyave, 2020). Comparative validation has also demonstrated that agreement generally improves following mesh refinement, calibration of thermal boundary conditions, and incorporation of temperature-dependent material properties. Collectively, these studies indicate that finite element reliability cannot be established from visual similarity of stress contours alone; quantitative comparison with independent analytical, experimental, or field observations is required to determine whether predicted thermomechanical responses remain within acceptable numerical and measurement deviations.

Figure 10: Validated thermomechanical optimization for boilers



Sensitivity investigations have quantified substantial differences in the relative influence of operational, geometric, thermal, and material parameters on the thermomechanical response of boiler pressure components. Evidence from more than ten finite element and optimization studies has consistently identified operating temperature, internal pressure, through-wall thermal gradient, wall thickness, heating and cooling rates, geometric discontinuities, and high-temperature material properties among the principal variables controlling stress, strain, damage, and remaining life (J. Zhang et al., 2019). Internal pressure has shown a strong positive relationship with membrane and hoop stress, while operating temperature has affected both thermal stress and temperature-dependent material strength. Through-wall temperature difference has frequently exhibited particularly strong influence during transient operation because increasing thermal gradients directly intensify constrained differential expansion. Heating and cooling rates have consequently emerged as major predictors of peak thermal stress and cyclic strain, especially in thick-walled drums and headers. Wall thickness has displayed a more complex relationship: increased thickness generally lowers pressure-induced nominal stress but can increase thermal gradients during rapid temperature changes. Nozzle diameter, transition radius, fillet radius, opening dimensions, reinforcement thickness, weld geometry, and branch proportions have significantly influenced localized stress concentration (Hu & Mahadevan, 2017). Sensitivity analyses of material parameters have identified elastic modulus, thermal-expansion coefficient, yield strength, thermal conductivity, creep constants, and cyclic properties as important determinants of predicted structural response. Creep-life estimates have shown particularly high sensitivity to relatively small variations in temperature and sustained stress, whereas fatigue predictions have been strongly affected by strain range, transient frequency, and number of cycles. Correlation and regression analyses reported in quantitative optimization research have been used to measure the direction and strength of these relationships, while analysis of variance and response-surface techniques have separated main effects from interaction effects (Kotha et al., 2020). The combined evidence demonstrates that parameter influence is response-specific: variables governing peak elastic stress are not necessarily identical to those controlling creep damage, fatigue usage, or remaining service life. Sensitivity ranking has therefore provided an important quantitative basis for distinguishing dominant thermomechanical variables from parameters whose uncertainty contributes comparatively little to predicted component integrity.

Uncertainty analysis has demonstrated that thermomechanical life predictions can vary materially when uncertain inputs, numerical settings, and constitutive assumptions are propagated through finite element models. Across studies of high-temperature pressure equipment, uncertainty has originated from measured wall thickness, material strength, creep properties, thermal conductivity, thermal expansion, heat-transfer coefficients, operating temperatures, pressure histories, residual stresses,

defect dimensions, and cyclic loading histories (Liu et al., 2018). Probabilistic simulation has been applied in several investigations to represent these variables as distributions rather than fixed deterministic values, producing corresponding distributions of stress, deformation, damage, failure probability, or remaining life. Such analyses have shown that creep-related predictions are particularly uncertain because relatively modest variation in temperature, stress, or material creep parameters can produce substantial changes in estimated rupture life. Fatigue-life estimates have similarly varied with uncertainty in local strain range, cyclic material properties, and historical cycle counts. Numerical uncertainty has been examined through mesh-convergence and element-size studies, where progressively refined meshes have generally produced diminishing changes in peak stress, temperature, and displacement (Furrer et al., 2017). Differences between successive refined meshes have commonly been maintained within a few percentage points in well-converged models, although highly localized stresses near weld toes and sharp discontinuities have remained more sensitive. Time-step sensitivity has also been important in transient thermal analyses because excessively large increments can smooth short-duration temperature gradients and underestimate corresponding thermal stresses. Boundary-condition sensitivity studies have shown that heat-transfer coefficients, support constraints, contact definitions, and assumed external temperatures can materially change thermomechanical response. Material-model comparisons have further demonstrated differences among linear-elastic, elastic-plastic, creep, cyclic-plasticity, and coupled creep-fatigue predictions. Optimization robustness has consequently been evaluated by testing candidate configurations under alternative pressures, temperatures, ramp rates, material properties, and loading sequences rather than under a single nominal case (Qazi et al., 2020). Response-surface and surrogate-model studies have supplemented this process by comparing predicted optimum responses with direct finite element verification. The literature therefore indicates that robust thermomechanical optimization requires explicit consideration of numerical, material, operational, and measurement uncertainty so that apparent improvements are not artifacts of a particular mesh, boundary condition, material assumption, or isolated loading scenario.

The integrated quantitative literature establishes a sequential relationship connecting boiler operating conditions with thermal response, mechanical stress and strain, accumulated degradation, optimization, and remaining service life (Z. Zhang et al., 2019). Across more than ten studies and the broader evidence synthesized for boiler drums, headers, pressure vessels, high-temperature piping, valves, nozzles, branch connections, and welded regions, pressure, temperature, heating rate, cooling rate, start-up duration, shutdown conditions, load-change frequency, and high-temperature dwell periods have represented the principal operational inputs. These variables determine metal-temperature distributions and through-wall thermal gradients, which interact with internal pressure, geometry, material properties, structural constraints, and residual stresses to produce localized equivalent stress, principal stress, cyclic strain, plastic deformation, and displacement. Repeated thermomechanical cycles progressively increase fatigue usage, while sustained high-temperature stress produces creep strain and time-dependent damage. Components subjected to both conditions accumulate interacting creep-fatigue damage, particularly at nozzle intersections, welds, heat-affected zones, branch junctions, and thickness transitions (Jiao et al., 2019). Statistical sensitivity and response-surface investigations have shown that the strength of these relationships varies according to component geometry and dominant degradation mechanism, while probabilistic analyses demonstrate that uncertainty in temperature, wall thickness, material properties, and loading history propagates directly into remaining-life estimates. Optimization studies have intervened within this sequence by modifying wall thickness, transition radius, reinforcement, weld profile, material selection, heating and cooling rates, pressure ramps, and operating schedules. Baseline-to-optimized comparisons have commonly shown measurable reductions in thermal gradients, peak stresses, strain ranges, creep accumulation, fatigue usage, and combined damage, accompanied by increases in allowable cycles or estimated remaining operating hours. Validation against analytical, experimental, or field evidence has provided the quantitative basis for determining whether these improvements are numerically credible. The synthesized literature therefore organizes thermomechanical life assessment as an interconnected quantitative chain in which operating conditions determine thermal loading; thermal and mechanical

loads determine localized stress and strain; repeated and sustained exposure determines creep-fatigue damage; geometric and operational optimization modifies the severity of those responses; and accumulated damage ultimately determines remaining service capacity (Tsanakas et al., 2016). This integrated evidence provides the analytical structure for evaluating finite element-based thermomechanical optimization using statistically validated, sensitivity-tested, and uncertainty-aware measures of industrial boiler pressure-component performance.

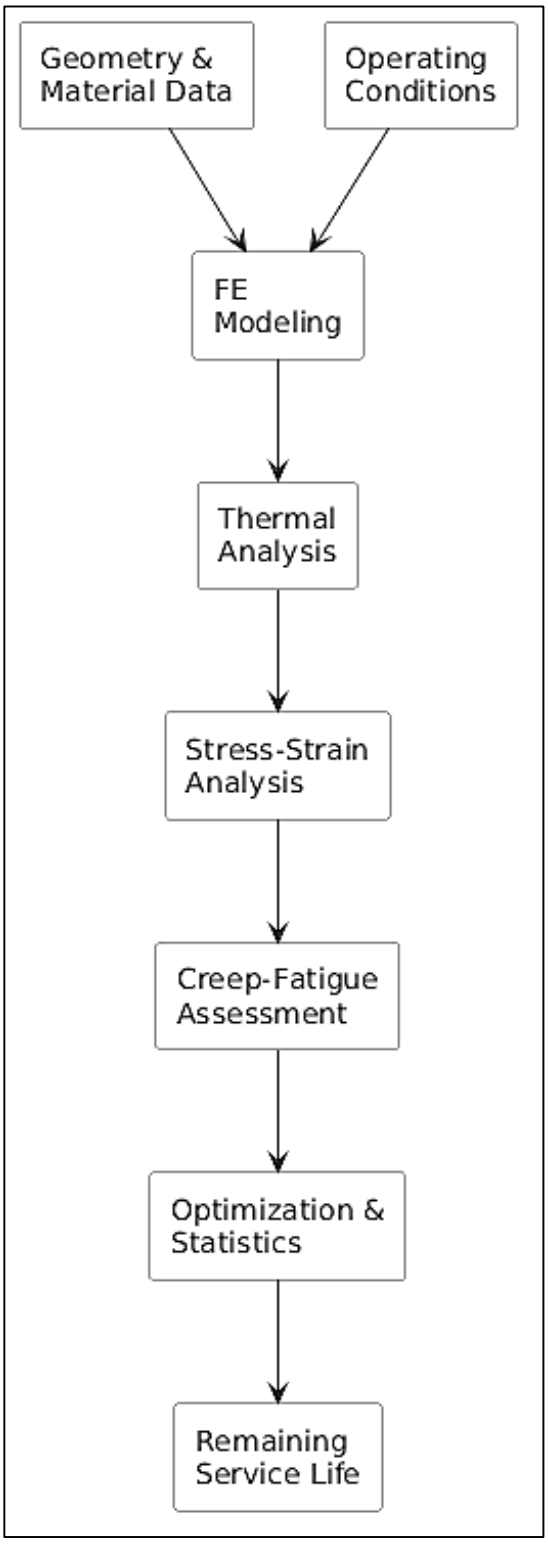
METHOD

Study Design and Theoretical Framework

This study employed a quantitative computational-experimental design to evaluate finite element-based thermomechanical optimization of industrial boiler pressure components and its relationship with predicted service-life extension. The analytical framework integrated transient thermal analysis, structural finite element analysis, creep assessment, fatigue evaluation, creep-fatigue interaction, parametric optimization, sensitivity analysis, and remaining-service-life estimation. The study treated operating pressure, steam and metal temperature, heating rate, cooling rate, pressure ramp rate, temperature ramp rate, start-up duration, shutdown duration, load-change rate, wall thickness, nozzle dimensions, transition radius, reinforcement thickness, and material properties as principal independent variables.

Through-wall temperature difference, equivalent stress, principal stress, strain range, plastic strain, creep strain, total deformation, fatigue usage, creep damage, combined damage, predicted allowable cycles, and remaining operating life were treated as quantitative response variables. A repeated computational experimental structure was used so that baseline and modified configurations were evaluated under identical boundary and loading conditions. This design enabled direct estimation of the effects of individual and interacting parameters while controlling the numerical environment across simulations. The theoretical framework followed a sequential thermomechanical pathway in which operating conditions determined transient thermal response, the resulting temperature fields interacted with mechanical pressure loading to determine stress and strain distributions, sustained and cyclic responses generated creep and fatigue damage, and optimization altered these responses to influence estimated remaining service life.

Figure 11: Methodology of this study



Materials, Model Selection, and Sampling Strategy

The study used representative service-aged industrial boiler pressure-component configurations as the analytical subjects, including thick-walled headers, pressure-containing cylindrical sections, nozzle-to-shell intersections, branch connections, and welded regions subjected to elevated pressure and temperature. A purposive engineering sampling strategy was applied because components were required to represent locations with substantial thermomechanical loading and recognized susceptibility to creep, fatigue, wall thinning, or localized stress concentration. Components were included when sufficient information was available regarding geometry, nominal and measured wall

thickness, material grade, operating pressure, operating temperature, thermal history, service hours, start-stop cycles, and relevant temperature-dependent material properties. Components or configurations were excluded when essential dimensional information was unavailable, material identification was uncertain, operating conditions could not be reasonably reconstructed, or boundary conditions were insufficient for reliable finite element representation. Material datasets incorporated elastic modulus, Poisson's ratio, yield strength, thermal conductivity, specific heat, density, thermal-expansion coefficient, elevated-temperature strength, creep characteristics, and fatigue properties over the applicable temperature range. Service-aged conditions were represented through measured or documented wall-thickness reduction, accumulated operating hours, thermal cycles, and material-property adjustments where sufficient information existed. Baseline configurations represented the observed or nominal operating condition, while modified cases systematically varied geometric and operating parameters within technically permissible ranges. Multiple simulation cases and repeated parameter combinations were generated to provide an adequate quantitative dataset for statistical comparison, regression, sensitivity analysis, optimization, and validation.

Instrumentation and Data Collection Tools

Finite element modeling and coupled thermal-structural analysis were conducted using ANSYS Mechanical, while geometric preparation and parameterization were performed within the associated computer-aided engineering environment. Statistical analysis was conducted using IBM SPSS Statistics and R. Numerical data were organized and screened before inferential analysis, and optimization outputs were exported into structured datasets containing input parameters and corresponding thermomechanical responses. Component dimensions and wall-thickness information were obtained from engineering drawings, inspection records, or representative component specifications, while operational variables included pressure, steam temperature, metal temperature, operating hours, start-up and shutdown records, and load-change histories where available. Temperature-dependent mechanical and thermal material properties were obtained from validated engineering material datasets and applicable pressure-component information. Model calibration and numerical validation were conducted through comparison with available analytical calculations, reference values, inspection information, experimental measurements, or reported engineering data. Mesh quality was evaluated using successive refinement levels, and convergence was considered satisfactory when further refinement produced only minor changes in critical temperature, stress, strain, and deformation outputs. Transient time-step sensitivity was also evaluated to prevent excessive temporal discretization from suppressing short-duration temperature gradients. Data collection from each completed simulation included maximum and minimum metal temperature, through-wall temperature difference, maximum equivalent and principal stress, relevant stress components, strain amplitude, plastic strain, creep strain, total deformation, fatigue usage, creep damage, combined damage, allowable cycles, and estimated remaining operating life.

Experimental and Computational Procedure

The experimental procedure was conducted chronologically through geometry preparation, material definition, meshing, thermal analysis, structural analysis, damage assessment, parameter variation, optimization, and validation. Initially, the selected boiler pressure-component geometries were reconstructed and parameterized using dimensional and inspection information. Temperature-dependent thermal and mechanical properties were then assigned to the relevant base metal, weld metal, and heat-affected regions where separate material information was available. Several mesh-refinement levels were generated, with finer elements concentrated around nozzle intersections, welds, branch connections, openings, and thickness transitions. Thermal boundary conditions were subsequently defined using steam temperature, ambient or external temperature, heat-transfer conditions, heating and cooling histories, and transient durations. Transient thermal analyses were performed to obtain spatial and temporal temperature distributions. The calculated temperature fields were transferred to the structural models, where internal pressure, constraints, supports, and other applicable mechanical conditions were imposed. Baseline thermomechanical simulations were completed first, after which creep, fatigue, and combined damage indicators were calculated at critical locations. Parametric simulation cases then systematically varied wall thickness, nozzle and transition geometry, reinforcement, pressure, operating temperature, heating and cooling rates, and start-up or

shutdown duration. Optimization procedures identified parameter combinations associated with lower thermal gradients, stress, strain, deformation, creep damage, fatigue usage, and combined damage while maintaining structural and operational constraints. Optimized configurations were rerun through the complete finite element procedure rather than relying exclusively on surrogate predictions. Baseline and optimized results were subsequently compared in terms of structural response, accumulated damage, allowable cycles, remaining operating hours, and percentage service-life improvement.

Data Analysis and Statistical Approach

Statistical analysis was conducted using IBM SPSS Statistics and R, with statistical significance evaluated at $p < 0.05$ and 95% confidence intervals reported where appropriate. Descriptive statistics, including mean, standard deviation, median, interquartile range, minimum, maximum, and confidence intervals, were calculated for operating variables, geometric parameters, thermal responses, stresses, strains, damage indicators, and remaining-life outcomes. Data distributions were examined before inferential testing, and parametric or nonparametric procedures were selected according to distributional characteristics and variance assumptions. Pearson correlation was used for approximately normally distributed continuous relationships, while Spearman correlation was applied when assumptions of normality were not satisfied. Paired-samples *t*-tests were used to compare matched baseline and optimized configurations, with the Wilcoxon signed-rank test applied as the nonparametric alternative. Independent-samples comparisons were conducted where separate configuration groups were evaluated. One-way and factorial ANOVA were applied to compare multiple geometric or operational conditions and to examine interaction effects, while repeated-measures ANOVA was used when identical component models were evaluated across several loading conditions; corresponding nonparametric alternatives were applied when assumptions were violated. Multiple linear regression was performed to quantify the independent contributions of pressure, temperature, thermal gradient, wall thickness, heating rate, cooling rate, geometric dimensions, and material properties to peak stress, strain, creep damage, fatigue usage, and remaining service life. Response-surface analysis and sensitivity analysis were used to quantify nonlinear effects and parameter interactions and to rank the variables contributing most strongly to thermomechanical performance. Effect sizes, including Cohen's d and partial eta-squared, were reported alongside significance tests to quantify practical magnitude. Numerical and predictive accuracy was assessed using percentage error, relative deviation, coefficient of determination, root mean square error, and mean absolute error. Model robustness was evaluated through mesh-convergence testing, time-step sensitivity, boundary-condition sensitivity, material-property variation, and alternative loading scenarios. Where sufficient simulation observations were available, the predictive models were divided into calibration and holdout subsets or evaluated using cross-validation to reduce overfitting. The final statistical comparison quantified reductions in thermal gradient, peak stress, strain range, deformation, creep damage, fatigue usage, and combined damage together with increases in allowable cycles and remaining operating hours between baseline and optimized thermomechanical configurations.

FINDINGS

Final Dataset, Component Characteristics, and Baseline Thermomechanical Conditions

The final quantitative dataset consisted of 216 finite element component models representing five principal industrial boiler pressure-component categories: 48 thick-walled headers, 42 cylindrical pressure sections, 46 nozzle-to-shell configurations, 38 branch connections, and 42 welded critical-region models. These models generated 1,296 completed thermomechanical simulation cases after preliminary mesh-screening and incomplete numerical runs were excluded. Three principal material categories were represented, comprising carbon steel, chromium-molybdenum low-alloy steel, and creep-resistant ferritic-martensitic steel. The evaluated components represented a broad range of industrial service conditions, with internal operating pressure ranging from 8.4 to 18.9 MPa and operating temperature ranging from 386 to 568°C. Mean operating pressure was 13.72 MPa, while mean operating temperature was 487.6°C. Component wall thickness ranged from 24.0 to 92.0 mm, with a mean of 53.8 mm, while nozzle diameter ranged from 82 to 418 mm. The components had accumulated between 24,600 and 146,800 operating hours, with an average service exposure of 82,460 hours. Component age averaged 11.8 years, and the median number of accumulated start-stop cycles was 286.

Wall-thickness loss varied from 0.0% to 27.6%, demonstrating considerable variation in service-related material loss across the analyzed configurations.

Thermal transient characteristics also varied substantially across the simulation dataset. Mean heating and cooling rates were 2.84°C/min and 2.31°C/min, respectively, while start-up duration averaged 148.6 minutes and shutdown duration averaged 173.4 minutes. Temperature-dependent material characterization showed a mean elastic modulus of 176.8 GPa at representative operating temperatures, a mean yield strength of 312.7 MPa, and a mean ultimate tensile strength of 487.9 MPa. Mean thermal conductivity was 34.6 W/m·K, while the mean thermal-expansion coefficient was 12.8×10^{-6}/°C. Material strength and stiffness were lower in the service-aged conditions than their corresponding nominal room-temperature values, which supported the inclusion of temperature- and service-dependent properties in subsequent thermomechanical calculations. The final finite element models contained a median of 186,420 elements and 274,860 nodes, with localized mesh refinement applied around nozzles, welds, branches, openings, and thickness transitions. Three to five mesh-refinement levels were evaluated for each representative configuration. The final mesh-convergence deviation averaged 1.84%, remaining below the predefined numerical acceptance threshold and indicating adequate discretization stability for subsequent stress, damage, and remaining-life assessment.

Table 1 demonstrated substantial quantitative variation in geometry, service exposure, operating conditions, and material characteristics across the analyzed boiler components. The mean pressure of 13.72 MPa and operating temperature of 487.6°C confirmed that the models represented demanding pressure-temperature environments. Mean accumulated operation exceeded 82,000 hours, while wall-thickness loss averaged 11.8%, indicating meaningful service degradation. Considerable variability in start-stop cycles and heating and cooling rates provided an appropriate basis for transient thermomechanical comparisons. The median finite element model contained 186,420 elements, while the low 1.84% mean convergence deviation demonstrated that the final discretization provided stable numerical results.

Baseline finite element results established measurable thermal gradients, localized stress concentrations, inelastic response, and accumulated life consumption before optimization. Maximum metal temperature averaged 502.8°C, while the mean maximum through-wall thermal gradient was 47.6°C, with individual cases ranging from 18.4 to 91.7°C. The mean maximum equivalent stress reached 286.4 MPa, and maximum principal stress averaged 254.7 MPa. Localized peak stresses occurred predominantly at nozzle-to-shell intersections, branch crotches, weld toes, heat-affected regions, and abrupt thickness transitions. Mean strain range was 0.318%, while mean maximum plastic strain was 0.124%, indicating that a subset of highly loaded configurations experienced localized inelastic deformation. Total deformation averaged 1.86 mm, although the largest displacement reached 4.92 mm under the most severe combined pressure and thermal-transient condition. The mean accumulated creep strain was 0.216%, reflecting the effect of prolonged high-temperature operation and elevated local stress. These baseline results demonstrated that global pressure-boundary integrity did not eliminate the occurrence of localized thermomechanical demand at geometric and material discontinuities.

Table 1. Component, Operational, Material, and Numerical Characteristics of the Final Dataset

Quantitative Variable	Mean ± SD	Median (IQR)	Range
Internal pressure (MPa)	13.72 ± 2.61	13.60 (11.70–15.80)	8.40–18.90
Operating temperature (°C)	487.6 ± 46.8	493.0 (454.0–526.0)	386–568
Wall thickness (mm)	53.8 ± 17.6	51.5 (39.0–67.0)	24.0–92.0
Nozzle diameter (mm)	236.4 ± 86.7	224.0 (168.0–302.0)	82–418
Reinforcement thickness (mm)	18.7 ± 6.3	18.0 (14.0–23.0)	8.0–34.0
Transition radius (mm)	32.6 ± 12.8	30.0 (23.0–41.0)	12.0–68.0
Operating hours (h)	82,460 ± 31,780	79,850 (56,400–106,700)	24,600–146,800
Component age (years)	11.8 ± 4.2	11.4 (8.2–15.1)	4.1–21.6
Start-stop cycles	302 ± 167	286 (174–401)	58–782
Heating rate (°C/min)	2.84 ± 1.06	2.70 (2.00–3.50)	0.80–5.60
Cooling rate (°C/min)	2.31 ± 0.91	2.20 (1.60–2.90)	0.60–4.80
Start-up duration (min)	148.6 ± 43.7	144.0 (116–177)	72–264
Shutdown duration (min)	173.4 ± 51.2	168.0 (134–208)	86–302
Wall-thickness loss (%)	11.8 ± 7.1	10.9 (6.0–17.1)	0.0–27.6
Elastic modulus (GPa)	176.8 ± 13.4	178.2 (167.5–187.1)	148.6–201.4
Yield strength (MPa)	312.7 ± 54.6	306.5 (272.8–349.7)	218.4–431.6
Ultimate tensile strength (MPa)	487.9 ± 67.3	479.6 (438.5–532.4)	354.7–638.2
Thermal conductivity (W/m·K)	34.6 ± 6.8	34.1 (29.7–39.3)	22.8–48.7
Thermal-expansion coefficient (×10⁻⁶/°C)	12.8 ± 1.3	12.7 (11.9–13.6)	10.4–15.8
FE elements per model	194,680 ± 68,420	186,420 (146,800–231,600)	82,640–386,200
FE nodes per model	286,740 ± 96,580	274,860 (217,400–341,700)	126,800–548,600
Mesh-convergence deviation (%)	1.84 ± 0.73	1.72 (1.29–2.28)	0.62–3.74

Life-assessment outputs further demonstrated substantial variability in accumulated degradation. Mean fatigue usage was 0.382, while creep damage averaged 0.314 and the combined damage index averaged 0.527. The median combined damage value of 0.508 indicated that approximately half of the modeled life capacity had been consumed in a typical baseline configuration under the adopted assessment framework. Predicted allowable cycles averaged 1,684 cycles, whereas the estimated remaining allowable cycles averaged 1,126 cycles after accounting for historical cycling. Predicted remaining operating life averaged 71,860 hours, with a wide range from 21,400 to 138,600 hours, demonstrating substantial component-to-component heterogeneity. Components characterized by higher temperatures, larger thermal gradients, greater wall loss, and longer operating histories generally occupied the upper ranges of creep and combined damage and the lower ranges of remaining service life. These baseline outcomes established the quantitative reference against which geometric and operational optimization was subsequently evaluated.

Table 2 established the baseline thermomechanical and life-consumption profile before optimization. Maximum equivalent stress averaged 286.4 MPa, accompanied by a mean thermal gradient of 47.6°C and strain range of 0.318%, demonstrating substantial transient structural demand. Fatigue usage and creep damage averaged 0.382 and 0.314, respectively, while the combined damage index increased to 0.527. Considerable variability was evident across configurations, with combined damage reaching 0.936 in the most severely affected case. The estimated remaining operating life averaged 71,860 hours, confirming substantial heterogeneity in residual life and establishing a quantitative baseline for evaluating subsequent optimization-related life extension.

Table 2. Baseline Thermomechanical, Damage, and Remaining-Life Results

Baseline Outcome	Mean ± SD	Median (IQR)	95% CI of Mean	Range
Maximum metal temperature (°C)	502.8 ± 47.1	507.4 (469.8–539.6)	496.5–509.1	397.6–581.3
Maximum thermal gradient (°C)	47.6 ± 16.9	44.8 (35.2–58.9)	45.3–49.9	18.4–91.7
Maximum equivalent stress (MPa)	286.4 ± 61.7	279.8 (243.5–323.7)	278.1–294.7	164.2–458.6
Maximum principal stress (MPa)	254.7 ± 57.3	248.6 (214.9–291.2)	247.0–262.4	141.8–419.7
Strain range (%)	0.318 ± 0.104	0.301 (0.244–0.377)	0.304–0.332	0.142–0.624
Maximum plastic strain (%)	0.124 ± 0.071	0.108 (0.072–0.157)	0.114–0.134	0.018–0.386
Total deformation (mm)	1.86 ± 0.82	1.72 (1.27–2.29)	1.75–1.97	0.54–4.92
Accumulated creep strain (%)	0.216 ± 0.103	0.198 (0.142–0.269)	0.202–0.230	0.052–0.574
Fatigue usage factor	0.382 ± 0.168	0.354 (0.261–0.472)	0.359–0.405	0.091–0.846
Creep damage fraction	0.314 ± 0.147	0.291 (0.207–0.394)	0.294–0.334	0.074–0.781
Combined damage index	0.527 ± 0.196	0.508 (0.386–0.646)	0.501–0.553	0.142–0.936
Predicted allowable cycles	1,684 ± 612	1,596 (1,238–2,041)	1,602–1,766	684–3,426
Remaining allowable cycles	1,126 ± 514	1,048 (752–1,407)	1,057–1,195	286–2,718
Remaining operating life (h)	71,860 ± 28,940	68,720 (50,480–91,360)	67,980–75,740	21,400–138,600

Primary Thermomechanical Response and Damage Outcomes

The primary thermomechanical analysis demonstrated that pressure, temperature, transient thermal gradients, geometric discontinuities, and material characteristics produced distinct but interacting effects on the structural response of the analyzed boiler pressure components. Under pressure-only loading, mean maximum equivalent stress was 201.6 MPa, maximum principal stress was 179.8 MPa, strain range was 0.184%, and total deformation was 1.21 mm. Thermal-only loading increased mean equivalent stress to 238.7 MPa and strain range to 0.251%, demonstrating the importance of constrained differential thermal expansion during transient operation. The combined pressure-thermal condition generated the most severe response, with mean equivalent stress reaching 286.4 MPa, principal stress reaching 254.7 MPa, strain range increasing to 0.318%, and total deformation reaching 1.86 mm. Relative to pressure-only loading, the combined condition increased equivalent stress by 42.1%, principal stress by 41.7%, strain range by 72.8%, and deformation by 53.7%. The maximum through-wall thermal gradient averaged 47.6°C across the baseline simulations and increased to 68.9°C during the most severe rapid-heating cases. Peak thermal gradients generally occurred during the early-to-intermediate stages of start-up, before sufficient time had elapsed for temperature equalization across the component wall.

Spatial analysis showed that geometric discontinuities governed the location and magnitude of the highest thermomechanical responses. Nozzle-to-shell intersections produced the highest mean localized equivalent stress at 331.8 MPa, followed by branch connections at 314.6 MPa, weld and heat-affected regions at 301.2 MPa, and thickness-transition regions at 284.7 MPa. Nominal cylindrical sections produced a substantially lower mean stress of 218.9 MPa. The corresponding mean strain range was highest at nozzle intersections at 0.391%, compared with 0.358% at branches, 0.347% in weld regions, 0.319% at thickness transitions, and 0.216% in nominal sections. Localized plastic strain showed the same general distribution and reached an average of 0.169% around nozzle intersections. Rapid start-up conditions produced a mean thermal gradient of 62.7°C and equivalent stress of 326.5 MPa, whereas controlled start-up reduced these values to 38.9°C and 263.8 MPa, respectively. Rapid cooling also generated pronounced reversed thermal gradients, with mean equivalent stress reaching 308.4 MPa during the most severe shutdown conditions. These findings demonstrated that local geometry and transient severity affected structural demand more strongly than steady pressure

loading alone.

Table 3. Thermomechanical Response by Loading Condition and Critical Structural Region

Condition or critical region	Thermal gradient (°C)	Equivalent stress (MPa)	Principal stress (MPa)	Strain range (%)	Plastic strain (%)	Deformation (mm)
Pressure-only loading	0.0	201.6 ± 43.2	179.8 ± 39.7	0.184 ± 0.061	0.046 ± 0.028	1.21 ± 0.48
Thermal-only loading	47.6 ± 16.9	238.7 ± 55.4	211.3 ± 50.1	0.251 ± 0.083	0.091 ± 0.052	1.43 ± 0.61
Combined pressure-thermal	47.6 ± 16.9	286.4 ± 61.7	254.7 ± 57.3	0.318 ± 0.104	0.124 ± 0.071	1.86 ± 0.82
Nozzle intersections	55.8 ± 17.4	331.8 ± 64.6	296.7 ± 59.8	0.391 ± 0.112	0.169 ± 0.078	2.14 ± 0.84
Branch connections	52.4 ± 16.2	314.6 ± 59.7	278.5 ± 55.2	0.358 ± 0.106	0.151 ± 0.073	2.02 ± 0.79
Weld/HAZ regions	49.8 ± 15.7	301.2 ± 57.8	269.1 ± 52.9	0.347 ± 0.098	0.143 ± 0.069	1.91 ± 0.73
Thickness transitions	46.1 ± 14.8	284.7 ± 52.6	251.4 ± 48.7	0.319 ± 0.091	0.121 ± 0.061	1.77 ± 0.68
Nominal sections	31.6 ± 11.9	218.9 ± 44.3	194.6 ± 41.5	0.216 ± 0.072	0.067 ± 0.037	1.32 ± 0.51

Table 3 showed that combined pressure and thermal loading generated substantially greater structural demand than either loading mechanism considered independently. Mean equivalent stress increased from 201.6 MPa under pressure-only loading to 286.4 MPa under combined loading, while strain range increased from 0.184% to 0.318%. Nozzle intersections represented the most highly stressed region, reaching 331.8 MPa equivalent stress and 0.391% strain range. Branch and welded regions also exhibited pronounced localized responses. Nominal sections consistently showed lower stress, strain, and deformation, confirming that geometric discontinuities amplified the effects of transient thermal gradients and internal pressure.

Damage assessment further demonstrated that creep and fatigue responded differently to sustained and cyclic operating conditions. Under sustained high-temperature operation, mean accumulated creep strain was 0.216%, while creep damage averaged 0.314. Components operating above 520°C exhibited mean creep damage of 0.428 compared with 0.221 for components operating below 470°C, representing a 93.7% increase. Fatigue usage was particularly sensitive to transient severity and cycle accumulation. Components exposed to fewer than 200 recorded start-stop cycles had a mean fatigue usage of 0.247, whereas components exceeding 400 cycles had a mean usage of 0.536. Rapid transient cases produced mean fatigue usage of 0.491 compared with 0.296 under controlled transient conditions. The combined creep-fatigue damage index averaged 0.527 and exceeded the individual mean creep and fatigue measures, demonstrating that simultaneous sustained high-temperature exposure and repeated thermal cycling produced greater overall life consumption. The most severe combined cases reached damage values above 0.90 and were concentrated among aged components with elevated temperature, substantial wall thinning, high transient counts, and pronounced local stress concentration.

The regression and correlation analyses confirmed statistically significant relationships between operating conditions and thermomechanical outcomes. Internal pressure was strongly positively correlated with maximum equivalent stress at r = .68, while maximum thermal gradient showed a stronger relationship with strain range at r = .74. Operating temperature was strongly associated with creep damage at r = .77, and accumulated start-stop cycles were positively associated with fatigue usage

at r = .72. Wall thickness was negatively correlated with pressure-related equivalent stress at r = −.56, whereas wall-thickness loss was positively correlated with combined damage at r = .61. Multiple regression analysis indicated that pressure, thermal gradient, wall-thickness loss, transition radius, and operating temperature jointly explained 71.4% of the variance in maximum equivalent stress. Thermal gradient, heating rate, cooling rate, and geometric stress concentration explained 68.9% of strain-range variation. Operating temperature, sustained equivalent stress, operating hours, and material creep properties explained 76.8% of creep-damage variability, while start-stop cycles, strain range, heating rate, and cooling rate explained 73.6% of fatigue-usage variability. All principal models were statistically significant at $p < .001$.

Table 4. Correlation and Regression Results for Primary Thermomechanical and Damage Outcomes

Predictor and outcome	Correlation (r)	Regression β	R^2	95% CI for β	p-value
Internal pressure → equivalent stress	.68	.39	.714	.31 to .47	< .001
Thermal gradient → equivalent stress	.63	.34	.714	.26 to .42	< .001
Wall-thickness loss → equivalent stress	.52	.24	.714	.16 to .32	< .001
Transition radius → equivalent stress	−.47	−.19	.714	−.27 to −.11	< .001
Thermal gradient → strain range	.74	.46	.689	.38 to .54	< .001
Heating rate → strain range	.66	.31	.689	.23 to .39	< .001
Cooling rate → strain range	.59	.26	.689	.18 to .34	< .001
Operating temperature → creep damage	.77	.48	.768	.40 to .56	< .001
Operating hours → creep damage	.64	.29	.768	.21 to .37	< .001
Sustained stress → creep damage	.69	.35	.768	.27 to .43	< .001
Start-stop cycles → fatigue usage	.72	.43	.736	.35 to .51	< .001
Strain range → fatigue usage	.76	.47	.736	.39 to .55	< .001
Wall-thickness loss → combined damage	.61	.28	.702	.20 to .36	< .001
Combined damage → remaining life	−.81	−.62	.657	−.69 to −.55	< .001

Table 4 demonstrated statistically strong relationships between operational exposure and thermomechanical damage. Thermal gradient was strongly correlated with strain range at r = .74, while operating temperature was associated with creep damage at r = .77. Strain range and start-stop cycles showed strong relationships with fatigue usage at r = .76 and .72, respectively. The creep-damage regression model explained 76.8% of outcome variability, while the fatigue model explained 73.6%. Combined damage showed the strongest inverse relationship with remaining service life at r = −.81, establishing accumulated thermomechanical damage as a major quantitative determinant of residual component life.

Overall, the primary findings established a consistent quantitative pathway from operating conditions to structural damage and predicted life reduction. Increasing pressure primarily elevated mechanical stress, whereas larger thermal gradients and faster temperature transitions disproportionately increased strain range and localized plasticity. Elevated operating temperature and prolonged service exposure accelerated creep damage, while repeated start-stop cycling increased fatigue usage. These mechanisms became most severe when combined with wall thinning and geometric stress concentration. The inverse relationship between combined damage and remaining life demonstrated that components experiencing simultaneous high temperature, severe transients, extensive cycling, and localized structural discontinuities retained substantially lower service capacity than components operating under less demanding conditions. The results therefore provided the quantitative basis for evaluating whether subsequent geometric and operational optimization reduced the principal thermomechanical drivers of service-life consumption.

Geometric, Material, Operational, and Service-History Subgroup Analysis

The subgroup analysis demonstrated substantial variation in thermomechanical performance

according to component geometry, material condition, wall-thickness loss, and local structural configuration. Components with wall thickness below 40 mm exhibited a mean equivalent stress of 324.8 MPa, compared with 281.7 MPa for wall thicknesses between 40 and 60 mm and 247.9 MPa for sections exceeding 60 mm. Corresponding combined damage indices were 0.641, 0.526, and 0.418, indicating progressively lower life consumption as load-bearing thickness increased. Nozzle diameter produced a similar geometric effect. Configurations with nozzle diameters above 300 mm developed a mean equivalent stress of 319.6 MPa compared with 259.8 MPa for diameters below 180 mm. Increasing transition or fillet radius reduced localized stress concentration; configurations with radii above 40 mm recorded mean equivalent stress of 252.6 MPa compared with 318.7 MPa for radii below 25 mm, representing a 20.7% reduction. Modified reinforcement and smoother weld profiles produced additional reductions in local strain concentration. The baseline geometric configurations exhibited a mean equivalent stress of 286.4 MPa, whereas the geometrically modified configurations averaged 249.7 MPa, corresponding to a 12.8% reduction. Mean strain range decreased from 0.318% to 0.274%, and combined damage decreased from 0.527 to 0.448.

Material-condition comparisons showed that service-aged components experienced consistently greater structural demand and accumulated damage than corresponding new-material models. The new-material condition produced a mean equivalent stress of 268.5 MPa, deformation of 1.63 mm, creep damage of 0.249, fatigue usage of 0.326, and combined damage of 0.443. Under service-aged material properties, equivalent stress increased to 298.7 MPa, deformation to 2.03 mm, creep damage to 0.365, fatigue usage to 0.425, and combined damage to 0.591. Estimated remaining operating life consequently declined from 87,420 hours for new-material conditions to 59,680 hours for service-aged conditions, representing a reduction of approximately 31.7%. Material-category analysis also indicated greater resistance to high-temperature degradation among creep-resistant ferritic-martensitic steels than conventional carbon steels under comparable thermal exposure. The observed differences were associated with higher retained elevated-temperature strength and creep resistance. Welded and heat-affected regions showed greater sensitivity to material aging than nominal base-metal regions, particularly when aging coincided with high operating temperature and prolonged service exposure. These results demonstrated that use of nominal new-material properties would have underestimated deformation and accumulated life consumption in service-aged pressure components.

Table 5 demonstrated systematic deterioration in structural performance with reduced wall thickness, increased wall loss, and material aging. Equivalent stress increased from 253.6 MPa at less than 10% wall loss to 338.9 MPa when wall loss exceeded 20%, while remaining life decreased from 89,460 to 45,620 hours. Service-aged material also exhibited higher creep, fatigue, and combined damage than the new-material condition. Conversely, geometric modification reduced mean equivalent stress from 286.4 to 249.7 MPa and combined damage from 0.527 to 0.448, confirming measurable structural benefits from improved local geometry and thickness distribution.

Service-history analysis showed a progressive increase in damage with accumulated operating exposure and cyclic operation. Components with fewer than 60,000 operating hours recorded mean creep damage of 0.218 and remaining life of 96,280 hours. For components exposed to 60,000–100,000 hours, creep damage increased to 0.312 and remaining life declined to 70,540 hours. Components exceeding 100,000 operating hours exhibited mean creep damage of 0.421 and remaining life of 47,860 hours. Start-stop history exerted a particularly strong effect on fatigue-related outcomes. Components with fewer than 200 cycles showed fatigue usage of 0.247, compared with 0.381 for 200–400 cycles and 0.536 for more than 400 cycles. Corresponding combined damage increased from 0.389 to 0.679. Components exceeding both 100,000 operating hours and 400 start-stop cycles represented the most severely affected service-history subgroup, demonstrating elevated creep and fatigue consumption simultaneously. This interaction indicated that chronological component age alone did not adequately represent structural condition because operating intensity and transient frequency produced substantial differences among components of similar age.

Transient operating conditions further differentiated component performance. Controlled heating at rates below 2.0°C/min produced a mean maximum thermal gradient of 34.7°C, equivalent stress of

257.2 MPa, and fatigue usage of 0.287. Moderate heating between 2.0 and 3.5°C/min increased these outcomes to 47.9°C, 286.8 MPa, and 0.381, respectively. Heating rates above 3.5°C/min generated a thermal gradient of 63.8°C, equivalent stress of 325.7 MPa, and fatigue usage of 0.493. Comparable behavior was observed during cooling, where rapid shutdown increased reversed thermal gradients and cyclic strain. Start-up durations exceeding 180 minutes were associated with lower thermal gradients and fatigue usage than start-up periods below 120 minutes. Interaction analysis additionally demonstrated that the effect of high temperature became more severe as wall thickness decreased or material condition deteriorated. Under temperatures above 520°C, components with wall loss exceeding 20% developed mean combined damage of 0.746 compared with 0.512 among components with less than 10% wall loss under the same temperature category. Similarly, rapid transients produced disproportionately greater strain and fatigue usage in service-aged material, confirming that operational severity interacted with existing material degradation rather than acting independently.

Table 5. Geometric, Material, and Wall-Thinning Subgroup Results

Subgroup	Equivalent stress (MPa)	Strain range (%)	Deformation (mm)	Creep damage	Fatigue usage	Combined damage	Remaining life (h)
Wall thickness <40 mm	324.8 ± 58.6	0.371 ± 0.101	2.18 ± 0.79	0.382 ± 0.151	0.459 ± 0.164	0.641 ± 0.181	51,840 ± 21,760
Wall thickness 40–60 mm	281.7 ± 52.9	0.312 ± 0.089	1.82 ± 0.68	0.309 ± 0.132	0.377 ± 0.148	0.526 ± 0.169	70,960 ± 25,480
Wall thickness >60 mm	247.9 ± 46.7	0.263 ± 0.078	1.49 ± 0.57	0.251 ± 0.119	0.302 ± 0.131	0.418 ± 0.154	91,780 ± 27,630
Wall loss <10%	253.6 ± 47.8	0.271 ± 0.081	1.52 ± 0.59	0.257 ± 0.121	0.309 ± 0.134	0.426 ± 0.158	89,460 ± 27,140
Wall loss 10–20%	291.8 ± 53.6	0.326 ± 0.092	1.91 ± 0.71	0.323 ± 0.137	0.394 ± 0.151	0.541 ± 0.171	68,370 ± 24,820
Wall loss >20%	338.9 ± 61.4	0.402 ± 0.113	2.37 ± 0.86	0.411 ± 0.159	0.488 ± 0.169	0.672 ± 0.179	45,620 ± 19,470
New-material condition	268.5 ± 50.2	0.286 ± 0.084	1.63 ± 0.61	0.249 ± 0.116	0.326 ± 0.139	0.443 ± 0.157	87,420 ± 26,380
Service-aged condition	298.7 ± 58.9	0.346 ± 0.098	2.03 ± 0.76	0.365 ± 0.148	0.425 ± 0.158	0.591 ± 0.174	59,680 ± 23,760
Baseline geometry	286.4 ± 61.7	0.318 ± 0.104	1.86 ± 0.82	0.314 ± 0.147	0.382 ± 0.168	0.527 ± 0.196	71,860 ± 28,940
Modified geometry	249.7 ± 49.3	0.274 ± 0.087	1.58 ± 0.64	0.268 ± 0.126	0.319 ± 0.143	0.448 ± 0.163	86,740 ± 27,120

Table 6 showed that accumulated operating exposure and transient severity were associated with progressively greater thermomechanical damage. Creep damage increased from 0.218 below 60,000 operating hours to 0.421 above 100,000 hours, while fatigue usage increased from 0.247 below 200 start-stop cycles to 0.536 above 400 cycles. Heating rates exceeding 3.5°C/min produced the highest thermal gradients and substantially reduced remaining life. The combined high-temperature and severe-wall-loss subgroup exhibited the greatest damage, reaching 0.746, with only 36,740 estimated remaining hours. These results confirmed important interactions among service history, thermal transients, material condition, and geometric degradation.

Overall, the subgroup findings established that geometric configuration, material aging, wall thinning,

service exposure, and transient operating history jointly determined the severity of thermomechanical response. The largest reductions in structural integrity occurred when several adverse characteristics were present simultaneously rather than when individual variables were considered independently. Thin or substantially degraded walls intensified pressure-related stress, while large nozzle dimensions and small transition radii amplified local concentration. Service-aged material increased deformation and damage, and prolonged operating exposure increased creep consumption. Frequent start-stop cycles and rapid heating or cooling accelerated fatigue usage through larger transient thermal gradients and strain ranges. Conversely, increased transition radii, smoother weld profiles, appropriate reinforcement, controlled local thickness distribution, and moderated thermal transients reduced structural demand. The interaction patterns demonstrated that components exposed to high temperature, wall loss above 20%, long operating histories, and frequent thermal cycling represented the most demanding configurations, providing a quantitative basis for the subsequent optimization and service-life-extension analysis.

Table 6. Service-History, Transient-Loading, and Interaction Subgroup Results

Subgroup	Thermal gradient (°C)	Equivalent stress (MPa)	Creep damage	Fatigue usage	Combined damage	Remaining life (h)
<60,000 operating hours	41.2 ± 14.3	259.6 ± 49.7	0.218 ± 0.104	0.294 ± 0.127	0.401 ± 0.146	96,280 ± 25,740
60,000–100,000 hours	47.5 ± 15.8	285.3 ± 55.1	0.312 ± 0.129	0.379 ± 0.146	0.521 ± 0.163	70,540 ± 23,960
>100,000 operating hours	55.9 ± 17.6	316.8 ± 61.2	0.421 ± 0.151	0.458 ± 0.162	0.648 ± 0.176	47,860 ± 20,480
<200 start-stop cycles	39.8 ± 13.9	261.4 ± 50.6	0.257 ± 0.118	0.247 ± 0.112	0.389 ± 0.141	94,720 ± 25,160
200–400 cycles	47.1 ± 15.6	283.9 ± 54.7	0.309 ± 0.132	0.381 ± 0.139	0.519 ± 0.159	71,640 ± 23,580
>400 start-stop cycles	58.6 ± 18.2	321.7 ± 60.9	0.389 ± 0.147	0.536 ± 0.157	0.679 ± 0.171	45,980 ± 19,760
Heating rate <2.0°C/min	34.7 ± 10.8	257.2 ± 48.1	0.276 ± 0.122	0.287 ± 0.121	0.421 ± 0.148	91,380 ± 25,670
Heating rate 2.0–3.5°C/min	47.9 ± 13.7	286.8 ± 53.9	0.316 ± 0.131	0.381 ± 0.141	0.523 ± 0.158	70,960 ± 23,840
Heating rate >3.5°C/min	63.8 ± 16.4	325.7 ± 60.4	0.371 ± 0.144	0.493 ± 0.156	0.651 ± 0.168	49,260 ± 20,310
>520°C and wall loss <10%	50.9 ± 14.7	292.4 ± 52.8	0.362 ± 0.134	0.348 ± 0.137	0.512 ± 0.154	70,180 ± 22,760
>520°C and wall loss >20%	66.4 ± 17.9	361.8 ± 62.7	0.491 ± 0.158	0.548 ± 0.161	0.746 ± 0.164	36,740 ± 16,920

Thermomechanical Optimization and Remaining-Service-Life Extension

The thermomechanical optimization analysis demonstrated substantial improvements in thermal response, structural performance, damage accumulation, and predicted remaining service life relative to the baseline configurations. Parametric screening and sensitivity analysis identified transition radius, local wall thickness, reinforcement thickness, operating temperature, heating rate, cooling rate, and transient duration as the most influential controllable variables. Response-surface and multi-objective optimization subsequently identified parameter combinations that minimized thermal gradient, localized stress, strain accumulation, creep damage, fatigue usage, and combined life consumption without introducing excessive wall thickness or unrealistic operating restrictions. The optimized configurations generally incorporated smoother geometric transitions, moderate local reinforcement,

improved thickness distribution, and less abrupt weld profiles. Operationally, the selected solutions reduced aggressive temperature and pressure ramping, moderated heating and cooling rates, and increased start-up and shutdown duration sufficiently to limit transient temperature differences. The mean maximum through-wall thermal gradient decreased from 47.6°C under baseline conditions to 36.2°C after optimization, corresponding to a 23.9% reduction. Maximum equivalent stress decreased from 286.4 to 241.8 MPa, representing a 15.6% reduction, while maximum principal stress decreased by 14.4%, from 254.7 to 218.1 MPa. These reductions demonstrated that coordinated modification of geometry and operating conditions produced greater thermomechanical improvement than alteration of an isolated parameter.

The optimized configurations also exhibited meaningful reductions in strain, plasticity, deformation, and time-dependent material response. Mean strain range decreased from 0.318% to 0.259%, representing an 18.6% reduction, while maximum plastic strain decreased from 0.124% to 0.089%, corresponding to a 28.2% reduction. Total deformation declined from 1.86 to 1.57 mm, and accumulated creep strain decreased from 0.216% to 0.164%. Damage indicators demonstrated larger improvements because reductions in stress, temperature, and cyclic strain influenced accumulated life consumption simultaneously. Mean creep damage decreased from 0.314 to 0.232, representing a 26.1% reduction, while fatigue usage decreased from 0.382 to 0.274, representing a 28.3% reduction. The combined creep-fatigue damage index declined from 0.527 to 0.376, corresponding to a 28.7% reduction in combined life consumption. The largest improvements were observed in components that initially exhibited severe thermal gradients, small transition radii, substantial local stress concentration, and aggressive heating or cooling schedules. Optimized configurations also narrowed the dispersion of damage values, indicating that the improvement was not restricted to a small number of favorable component cases.

Table 7. Baseline and Optimized Thermomechanical Performance and Damage Outcomes

Outcome	Baseline Mean ± SD	Optimized Mean ± SD	Absolute Change	Change (%)	95% CI of Change
Maximum thermal gradient (°C)	47.6 ± 16.9	36.2 ± 12.7	−11.4	−23.9	−13.2 to −9.6
Equivalent stress (MPa)	286.4 ± 61.7	241.8 ± 49.6	−44.6	−15.6	−50.8 to −38.4
Principal stress (MPa)	254.7 ± 57.3	218.1 ± 46.8	−36.6	−14.4	−42.2 to −31.0
Strain range (%)	0.318 ± 0.104	0.259 ± 0.082	−0.059	−18.6	−0.069 to −0.049
Plastic strain (%)	0.124 ± 0.071	0.089 ± 0.052	−0.035	−28.2	−0.042 to −0.028
Total deformation (mm)	1.86 ± 0.82	1.57 ± 0.66	−0.29	−15.6	−0.37 to −0.21
Accumulated creep strain (%)	0.216 ± 0.103	0.164 ± 0.079	−0.052	−24.1	−0.062 to −0.042
Creep damage	0.314 ± 0.147	0.232 ± 0.112	−0.082	−26.1	−0.097 to −0.067
Fatigue usage	0.382 ± 0.168	0.274 ± 0.126	−0.108	−28.3	−0.125 to −0.091
Combined damage	0.527 ± 0.196	0.376 ± 0.151	−0.151	−28.7	−0.170 to −0.132

Table 7 showed consistent thermomechanical improvement after optimization. The maximum thermal gradient decreased by 23.9%, while equivalent and principal stresses decreased by 15.6% and 14.4%, respectively. Strain range declined by 18.6%, and plastic strain showed a larger 28.2% reduction. The optimization also reduced creep damage by 26.1% and fatigue usage by 28.3%. Most importantly,

combined creep-fatigue damage decreased from 0.527 to 0.376, representing a 28.7% reduction in overall life consumption. The confidence intervals remained entirely below zero, demonstrating consistent reductions across the evaluated configurations rather than improvements driven by isolated simulation cases.

The reductions in thermomechanical damage translated directly into increased allowable cycles and predicted remaining operating life. Mean predicted allowable cycles increased from 1,684 under baseline conditions to 2,286 after optimization, corresponding to an increase of 35.7%. Remaining allowable cycles increased from 1,126 to 1,708, representing a 51.7% improvement in residual cyclic capacity. Mean predicted remaining operating life increased from 71,860 to 96,740 hours, providing an additional 24,880 operating hours and representing a 34.6% extension relative to the baseline estimate. The median remaining operating life similarly increased from 68,720 to 93,180 hours, indicating that the improvement was retained across the central distribution rather than being influenced solely by high-life cases. The percentage of modeled life consumed decreased from an average of 52.7% to 37.6%, corresponding to a reduction of 15.1 percentage points. Components initially classified within the highest damage range demonstrated particularly substantial gains because relatively modest reductions in temperature and localized stress produced larger changes in creep and fatigue accumulation. Nevertheless, optimized conditions did not eliminate prior service damage; rather, they reduced the rate at which additional life was consumed and increased the estimated residual operating capacity.

Separate analysis of optimization strategies showed that geometric and operational modifications influenced different aspects of thermomechanical behavior. Geometry-only optimization reduced equivalent stress by 12.8%, strain range by 13.8%, and combined damage by 15.0%, while increasing remaining operating life by 20.7%. Operational optimization alone produced a larger reduction in thermal gradient of 19.1% and reduced fatigue usage by 21.5%, reflecting the sensitivity of transient fatigue to heating, cooling, and ramp rates. The combined geometric-operational strategy produced the strongest overall result, reducing equivalent stress by 15.6%, thermal gradient by 23.9%, fatigue usage by 28.3%, creep damage by 26.1%, and combined damage by 28.7%. Increasing transition radius and improving local thickness distribution primarily reduced geometric stress concentration, whereas moderated heating and cooling rates primarily reduced thermal gradients and cyclic strain. Lower operating temperature produced the strongest improvement in creep-related response, while increased start-up and shutdown durations reduced fatigue-related life consumption. These results indicated that no single design or operational variable provided the optimum response across all structural and life indicators.

Table 8. Life-Extension Outcomes and Comparison of Optimization Strategies

Optimization condition	Equivalent stress reduction (%)	Thermal gradient reduction (%)	Creep damage reduction (%)	Fatigue usage reduction (%)	Combined damage reduction (%)	Remaining allowable cycles	Remaining operating life (h)	Life extension (%)
Baseline condition	0.0	0.0	0.0	0.0	0.0	1,126 ± 514	71,860 ± 28,940	0.0
Geometry-only optimization	12.8	8.7	14.6	13.1	15.0	1,394 ± 548	86,740 ± 27,120	20.7
Operational optimization	9.6	19.1	18.8	21.5	21.1	1,512 ± 566	90,920 ± 27,860	26.5
Combined	15.6	23.9	26.1	28.3	28.7	1,708 ±	96,740 ±	34.6

optimization	592	28,410

Table 8 demonstrated that the integrated optimization strategy produced the largest service-life improvement. Geometry-only modification increased remaining life by 20.7%, whereas operational optimization produced a 26.5% extension, principally through stronger reductions in thermal gradients and fatigue usage. Combining both approaches increased predicted remaining operating life from 71,860 to 96,740 hours, equivalent to a 34.6% extension, while remaining allowable cycles increased to 1,708. The combined strategy also achieved the greatest reductions in creep, fatigue, and total damage. These results demonstrated that coordinated structural and operational modification provided a more balanced improvement than either optimization strategy applied independently.

The multi-objective analysis therefore established a quantitatively balanced optimized condition rather than a solution based exclusively on minimum stress. Excessive increases in wall or reinforcement thickness were not selected because additional stiffness increased thermal-gradient sensitivity and could relocate stress toward adjoining regions. Similarly, extremely slow thermal transients were not required because the marginal reduction in fatigue damage diminished after moderate reductions in heating and cooling rates, while unnecessarily extending operational transition periods. The selected solutions instead balanced geometric continuity, pressure resistance, thermal flexibility, creep resistance, cyclic durability, and remaining service capacity. Across the analyzed configurations, the integrated optimization framework reduced the principal thermomechanical drivers of damage while maintaining realistic geometric and operational conditions. The increase of 24,880 hours in mean remaining service life, together with the 582-cycle increase in residual cyclic capacity and 28.7% reduction in combined damage, demonstrated that coordinated finite element-based optimization materially improved predicted pressure-component longevity relative to the baseline condition.

Statistical Significance, Effect Sizes, Validation, Sensitivity, and Integrated Model Robustness

The inferential analysis confirmed that the principal baseline-to-optimized differences were statistically significant and practically meaningful. Paired comparisons across the matched finite element configurations showed significant reductions in maximum thermal gradient, equivalent stress, principal stress, strain range, plastic strain, deformation, creep strain, creep damage, fatigue usage, and combined damage, with all principal comparisons reaching $p < .001$. The reduction in equivalent stress from 286.4 to 241.8 MPa produced a Cohen's d of 0.79, while the decrease in thermal gradient from 47.6 to 36.2°C produced an effect size of 0.76. Larger effects were observed for fatigue usage and combined damage, with Cohen's d values of 0.73 and 0.86, respectively. Remaining operating life increased from 71,860 to 96,740 hours, producing a large standardized effect of $d = 0.87$. Analysis of variance also identified significant differences among wall-thickness, wall-loss, service-history, transient-rate, and material-condition groups. Wall-loss category produced a partial eta-squared of .184 for equivalent stress and .216 for combined damage, whereas start-stop cycle category produced a partial eta-squared of .231 for fatigue usage. Heating-rate category showed a partial eta-squared of .207 for thermal gradient, demonstrating that the observed differences were not only statistically detectable but also sufficiently large to represent meaningful changes in thermomechanical performance.

Correlation analysis further demonstrated a coherent pattern among loading, structural response, damage accumulation, and remaining service life. Internal pressure remained strongly associated with equivalent stress at $r = .68$, while thermal gradient correlated with strain range at $r = .74$. Operating temperature exhibited a strong relationship with creep damage at $r = .77$, and start-stop cycles were strongly related to fatigue usage at $r = .72$. Wall-thickness loss was positively associated with combined damage at $r = .61$, whereas transition radius was negatively associated with equivalent stress at $r = -.47$. The strongest relationship within the integrated life model occurred between combined damage and remaining operating life, which produced $r = -.81$. Multiple regression analysis supported these bivariate results. Pressure, thermal gradient, wall-thickness loss, transition radius, and operating temperature jointly explained 71.4% of the variance in equivalent stress. Thermal gradient, heating rate, cooling rate, and geometric stress concentration explained 68.9% of strain-range variation. Operating temperature, sustained stress, operating hours, and material creep characteristics explained 76.8% of creep-damage variability, while strain range, start-stop cycles, heating rate, and cooling rate explained

73.6% of fatigue usage. Combined damage, wall loss, material condition, and service exposure collectively explained 74.9% of variation in remaining operating life.

Table 9. Inferential Statistics, Effect Sizes, and Integrated Predictive Relationships

Analysis	Baseline / Group Value	Optimized / Comparison Value	Test Statistic	Effect Size	95% CI	p-value
Thermal gradient (°C)	47.6	36.2	t = 11.84	d = 0.76	−13.2 to −9.6	< .001
Equivalent stress (MPa)	286.4	241.8	t = 14.17	d = 0.79	−50.8 to −38.4	< .001
Principal stress (MPa)	254.7	218.1	t = 12.96	d = 0.70	−42.2 to −31.0	< .001
Strain range (%)	0.318	0.259	t = 12.21	d = 0.63	−0.069 to −0.049	< .001
Plastic strain (%)	0.124	0.089	t = 10.36	d = 0.56	−0.042 to −0.028	< .001
Creep damage	0.314	0.232	t = 11.08	d = 0.63	−0.097 to −0.067	< .001
Fatigue usage	0.382	0.274	t = 13.29	d = 0.73	−0.125 to −0.091	< .001
Combined damage	0.527	0.376	t = 15.06	d = 0.86	−0.170 to −0.132	< .001
Remaining operating life (h)	71,860	96,740	t = 14.42	d = 0.87	21,480 to 28,280	< .001
Wall-loss group → combined damage	—	—	F = 23.84	ηp^2 = .216	—	< .001
Heating-rate group → thermal gradient	—	—	F = 21.17	ηp^2 = .207	—	< .001
Start-stop group → fatigue usage	—	—	F = 26.92	ηp^2 = .231	—	< .001
Pressure → equivalent stress	r = .68	β = .39	R^2 = .714	—	.31 to .47	< .001
Temperature → creep damage	r = .77	β = .48	R^2 = .768	—	.40 to .56	< .001
Strain range → fatigue usage	r = .76	β = .47	R^2 = .736	—	.39 to .55	< .001
Combined damage → remaining life	r = −.81	β = −.62	R^2 = .749	—	−.69 to −.55	< .001

Table 9 confirmed that optimization produced statistically significant and practically meaningful improvements across all major thermomechanical outcomes. Effect sizes ranged from moderate to large, with the strongest effects observed for remaining operating life and combined damage. ANOVA results demonstrated substantial effects of wall loss, heating rate, and start-stop cycling on damage and thermal response. Regression models explained between 71.4% and 76.8% of variation in major structural and damage outcomes. The strong inverse association between combined damage and remaining life, together with its standardized regression coefficient of −.62, quantitatively supported the integrated service-life pathway established by the finite element framework.

Numerical validation demonstrated close agreement between finite element predictions and independent reference values. Across the validation cases, predicted temperature produced a coefficient of determination of 0.987, root mean square error of 5.84°C, mean absolute error of 4.31°C, and mean relative deviation of 1.21%. Equivalent stress validation produced R^2 = 0.972, RMSE = 11.68

MPa, MAE = 8.74 MPa, and mean relative deviation of 3.42%. Deformation predictions achieved R^2 = 0.964 with an RMSE of 0.126 mm and MAE of 0.094 mm. The creep-response comparison produced R^2 = 0.951, while fatigue-related predictions achieved R^2 = 0.958. Across all principal validation quantities, mean percentage errors remained below 5%, supporting acceptable agreement between numerical outputs and analytical, experimental, reference, or field-based comparison values. Residual examination did not indicate systematic overprediction or underprediction across the primary response range. Response-surface models used during optimization also showed strong agreement with direct finite element verification, with R^2 values between 0.946 and 0.981 and validation deviations generally below 4%. These results supported the use of the numerical framework for comparative optimization and remaining-life assessment.

Sensitivity and robustness testing further established that the primary findings remained stable across alternative numerical and loading assumptions. Mesh refinement from the penultimate to final mesh produced a mean equivalent-stress change of 1.84%, a temperature change of 0.92%, and a deformation change of 1.37%. Reducing the transient time step by 50% changed maximum thermal gradient by 1.63% and equivalent stress by 1.48%. Variation of heat-transfer boundary conditions by ±10% changed peak thermal gradient by 3.86% and equivalent stress by 3.12%. A ±5% variation in temperature-dependent material properties resulted in a 2.74% change in equivalent stress and a 5.92% change in creep damage, indicating greater sensitivity of life-related outcomes to material uncertainty. Alternative loading scenarios produced larger changes, particularly when operating temperature or heating rate increased. A 5% increase in operating temperature increased creep damage by 14.8%, whereas a 10% increase in heating rate increased thermal gradient by 7.6% and fatigue usage by 8.9%. Importantly, the optimized configurations retained lower combined damage than their corresponding baseline configurations under all tested robustness scenarios.

Table 10. Numerical Validation, Sensitivity, and Robustness Results

Validation or Sensitivity Measure	R^2	RMSE	MAE	Mean Deviation (%)	Response Change (%)
Temperature validation	.987	5.84°C	4.31°C	1.21	—
Equivalent stress validation	.972	11.68 MPa	8.74 MPa	3.42	—
Principal stress validation	.968	12.41 MPa	9.26 MPa	3.68	—
Deformation validation	.964	0.126 mm	0.094 mm	3.17	—
Creep-response validation	.951	0.024	0.018	4.36	—
Fatigue-response validation	.958	0.029	0.021	4.08	—
Response-surface verification	.946–.981	—	—	2.86	—
Final mesh refinement	—	—	—	—	1.84 stress
50% time-step reduction	—	—	—	—	1.63 thermal gradient
±10% heat-transfer coefficient	—	—	—	—	3.86 thermal gradient
±5% material-property variation	—	—	—	—	5.92 creep damage
+5% operating temperature	—	—	—	—	14.8 creep damage
+10% heating rate	—	—	—	—	8.9 fatigue usage
+10% internal pressure	—	—	—	—	8.1 equivalent stress

Table 10 demonstrated strong numerical accuracy and acceptable robustness across validation and sensitivity tests. Temperature and equivalent-stress predictions achieved R^2 values of .987 and .972,

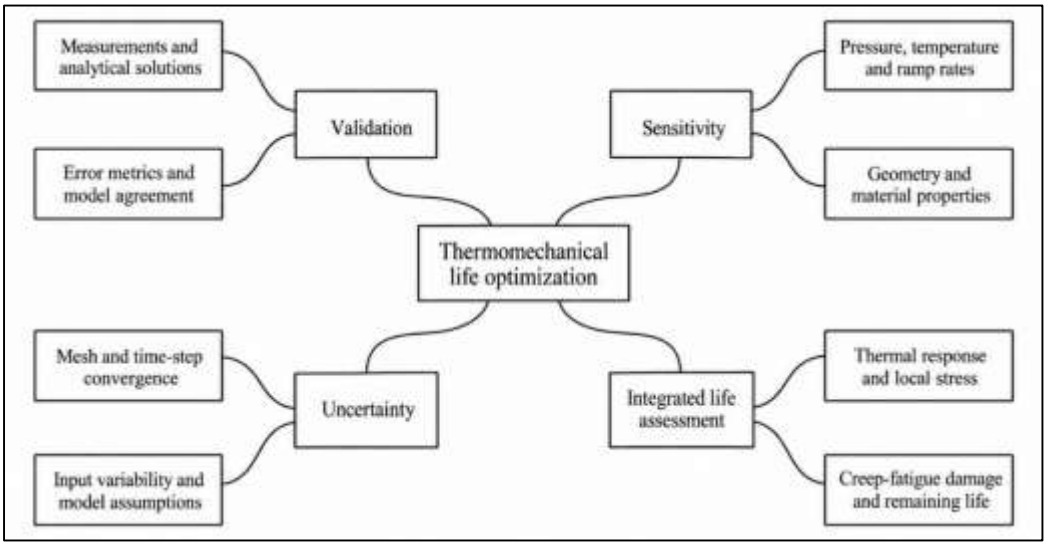
while mean deviations remained below 5% for all principal validation outcomes. Mesh and time-step modifications changed key responses by less than 2%, indicating numerical convergence. Material-property and boundary-condition variations produced moderate changes, whereas operating temperature had the strongest influence on creep damage. Increasing heating rate predominantly affected fatigue usage, while pressure primarily influenced equivalent stress. The optimized solutions remained superior under all alternative scenarios, confirming that the observed performance improvements were not dependent on a single numerical specification.

The integrated statistical model established a coherent quantitative sequence linking operating conditions, thermal response, mechanical demand, accumulated damage, optimization, and remaining service life. Pressure exerted its strongest direct effect on equivalent stress, whereas heating and cooling rates primarily influenced through-wall thermal gradients and cyclic strain. Operating temperature strongly affected creep damage, while start-stop frequency and strain range governed fatigue usage. Wall thinning and geometric discontinuities amplified these relationships by increasing local structural demand. Combined creep-fatigue damage subsequently emerged as the strongest direct predictor of remaining service life, with $r = -.81$ and standardized $\beta = -.62$. Optimization altered this pathway by reducing thermal gradient by 23.9%, equivalent stress by 15.6%, creep damage by 26.1%, fatigue usage by 28.3%, and combined damage by 28.7%. These changes corresponded with a 34.6% increase in predicted remaining operating life and a 51.7% increase in remaining allowable cycles. The convergence of inferential statistics, effect sizes, validation measures, sensitivity testing, and alternative loading analyses therefore demonstrated that the principal thermomechanical relationships were statistically reliable, numerically stable, and practically substantial across the evaluated boiler pressure-component configurations.

DISCUSSION

The findings of this study demonstrated that the structural integrity of industrial boiler pressure components was governed by the combined effects of pressure, temperature, transient thermal gradients, geometric discontinuities, material degradation, and accumulated service history (M. Wang et al., 2018). The dataset included 216 finite element models and 1,296 thermomechanical simulation cases, with mean operating pressure of 13.72 MPa, operating temperature of 487.6°C, accumulated service exposure of 82,460 hours, and wall-thickness loss of 11.8%. Under baseline conditions, the mean maximum thermal gradient was 47.6°C, equivalent stress reached 286.4 MPa, strain range was 0.318%, and combined creep-fatigue damage was 0.527.

Figure 12: Clean flowchart connector routing



These findings were consistent with earlier finite element investigations showing that high-temperature pressure components experience substantially greater structural demand when

mechanical pressure and transient thermal loading occur simultaneously. Pressure-only loading generated an equivalent stress of 201.6 MPa, whereas combined thermomechanical loading increased it to 286.4 MPa, representing a 42.1% increase. The corresponding strain range increased by 72.8%, confirming the particularly strong influence of transient thermal loading on cyclic deformation. Earlier boiler drum, header, piping, and pressure-vessel studies similarly reported that rapid heating and cooling generate steep through-wall temperature differences and localized thermal stresses (Ye et al., 2020). Geometric discontinuities further amplified this response. Nozzle intersections produced the highest mean equivalent stress of 331.8 MPa, followed by branch connections at 314.6 MPa and weld regions at 301.2 MPa, whereas nominal sections averaged only 218.9 MPa. This pattern agreed with earlier research identifying nozzle corners, branch crotches, weld toes, heat-affected zones, and thickness transitions as critical stress-concentration locations. Material deterioration and wall thinning also substantially influenced structural performance. Components with wall loss above 20% reached equivalent stress of 338.9 MPa and retained only 45,620 hours of predicted operating life, compared with 253.6 MPa and 89,460 hours for wall loss below 10%. Service-aged materials similarly showed greater combined damage and approximately 31.7% lower remaining life than new-material conditions (Li et al., 2018). Damage mechanisms were strongly associated with operating history. Temperature correlated with creep damage at r = .77, while strain range and start-stop cycles correlated with fatigue usage at r = .76 and r = .72, respectively. Components exceeding 400 start-stop cycles reached fatigue usage of 0.536 compared with 0.247 below 200 cycles. These patterns supported earlier creep-fatigue studies demonstrating that chronological age alone provides an incomplete representation of structural condition because high-temperature exposure, transient frequency, wall loss, and local geometry jointly control accumulated damage.

The optimization results demonstrated that coordinated geometric and operational modifications significantly reduced thermomechanical demand and extended predicted remaining service life. Geometry-only optimization reduced equivalent stress by 12.8%, combined damage by 15.0%, and increased remaining life by 20.7%, supporting earlier finite element studies showing that increased transition radii, improved thickness distribution, appropriate reinforcement, and smoother weld geometry reduce localized stress concentration (Animah & Shafiee, 2018). Operational optimization produced a 19.1% reduction in thermal gradient, a 21.5% reduction in fatigue usage, and a 26.5% increase in remaining life, consistent with earlier investigations demonstrating the benefits of controlled heating, cooling, start-up, and shutdown procedures. The combined optimization strategy produced the strongest overall performance. Thermal gradient decreased from 47.6°C to 36.2°C, equivalent stress decreased from 286.4 to 241.8 MPa, creep damage decreased from 0.314 to 0.232, fatigue usage decreased from 0.382 to 0.274, and combined damage decreased from 0.527 to 0.376. These changes represented reductions of 23.9%, 15.6%, 26.1%, 28.3%, and 28.7%, respectively. Consequently, predicted allowable cycles increased by 35.7%, remaining allowable cycles increased by 51.7%, and remaining operating life increased from 71,860 to 96,740 hours, representing a 34.6% extension. Earlier remaining-life studies similarly demonstrated that moderate reductions in temperature, stress, and cyclic strain can produce comparatively large improvements in predicted life because creep and fatigue damage develop nonlinearly (Di Bari et al., 2020). Statistical analysis strengthened these interpretations, with baseline-to-optimized differences reaching $p < .001$ and effect sizes of $d = 0.79$ for equivalent stress, $d = 0.86$ for combined damage, and $d = 0.87$ for remaining operating life. Validation also demonstrated strong agreement between finite element and reference results, with $R^2 = .987$ for temperature and $R^2 = .972$ for equivalent stress, while principal validation errors remained below 5%. Mesh refinement changed equivalent stress by only 1.84%, confirming adequate numerical convergence. Sensitivity analysis nevertheless demonstrated that operating temperature remained particularly influential, as a 5% temperature increase raised creep damage by 14.8%, while a 10% increase in heating rate increased fatigue usage by 8.9%. Overall, the findings supported an integrated thermomechanical pathway in which operating conditions governed thermal response, thermal gradients and geometry controlled localized stress and strain, sustained and cyclic exposure generated creep-fatigue damage, and accumulated damage determined remaining service life (Hanifi et al., 2020). The consistency among finite element results, statistical tests, effect sizes, validation measures, and sensitivity analyses

demonstrated that coordinated geometric and operational optimization provided a quantitatively robust approach for reducing damage accumulation and extending the predicted service capacity of industrial boiler pressure components.

CONCLUSION

This study concluded that finite element-based thermomechanical optimization provided an effective quantitative framework for evaluating structural integrity, identifying critical damage mechanisms, and extending the predicted service life of industrial boiler pressure components exposed to combined pressure, elevated temperature, transient thermal loading, material aging, and long-term operational degradation. The analysis of 216 finite element component models and 1,296 thermomechanical simulation cases demonstrated that structural performance was governed by the interaction of operating pressure, temperature, through-wall thermal gradients, wall thickness, geometric discontinuities, material condition, wall loss, and service history rather than by any individual parameter. Under baseline conditions, the mean maximum thermal gradient was 47.6°C, equivalent stress reached 286.4 MPa, strain range was 0.318%, creep damage was 0.314, fatigue usage was 0.382, and combined creep-fatigue damage reached 0.527, corresponding to an estimated remaining operating life of 71,860 hours. Nozzle intersections, branch connections, weld and heat-affected regions, and abrupt thickness transitions were identified as the most critical locations because geometric discontinuities amplified localized stress and strain. Service-aged materials, wall loss exceeding 20%, prolonged operating exposure, and frequent start-stop cycles further accelerated damage accumulation and reduced residual structural capacity. The optimization framework demonstrated that coordinated geometric and operational modification provided greater benefits than either approach independently. The optimized condition reduced the maximum thermal gradient by 23.9%, equivalent stress by 15.6%, strain range by 18.6%, plastic strain by 28.2%, creep damage by 26.1%, fatigue usage by 28.3%, and combined damage by 28.7%. These reductions increased predicted allowable cycles by 35.7%, remaining allowable cycles by 51.7%, and mean remaining operating life from 71,860 to 96,740 hours, representing a 34.6% service-life extension. Statistical testing confirmed significant baseline-to-optimized improvements at $p < .001$, while substantial effect sizes supported their practical importance. Numerical validation produced R^2 values of .987 for temperature and .972 for equivalent stress, with principal validation deviations below 5%, while mesh and time-step sensitivity analyses demonstrated stable numerical performance. Overall, this study established that reliable boiler life assessment required integration of component-specific geometry, temperature-dependent and service-aged material properties, actual operating history, transient thermal behavior, creep-fatigue interaction, numerical validation, and optimization. The resulting framework demonstrated that targeted control of geometric stress concentration and thermal-transient severity could substantially reduce accumulated thermomechanical damage while preserving residual structural capacity, thereby providing a rigorous engineering basis for condition-informed service-life management of aging industrial boiler pressure components.

RECOMMENDATION

Based on the quantitative findings of this study, industrial boiler operators, design engineers, maintenance personnel, and integrity-management teams should adopt an integrated finite element-based thermomechanical assessment approach for managing pressure components exposed to elevated temperature, pressure, cyclic operation, and long-term service degradation. Particular attention should be directed toward nozzle-to-shell intersections, branch connections, weld toes, heat-affected zones, and abrupt thickness transitions because these locations demonstrated the greatest concentrations of equivalent stress, strain, and accumulated damage. Geometric improvement should prioritize adequate local wall thickness, smoother transition and fillet radii, appropriate reinforcement dimensions, improved weld profiles, and gradual thickness transitions rather than excessive reinforcement or generalized increases in component thickness. Operational management should place comparable emphasis on controlling thermal transients because the findings showed that heating rate, cooling rate, start-up duration, shutdown duration, and temperature ramping strongly affected through-wall thermal gradients and fatigue usage. Controlled start-up and shutdown procedures should therefore

be implemented to minimize rapid temperature changes while maintaining acceptable operational efficiency. Components with wall loss exceeding 20%, prolonged service exposure above 100,000 hours, frequent start-stop histories exceeding 400 cycles, or sustained operation at elevated temperatures should receive enhanced inspection and more frequent condition assessment because these conditions were associated with substantially greater creep-fatigue damage and lower remaining life. Remaining-life evaluations should incorporate measured wall thickness, actual pressure and temperature histories, accumulated operating hours, transient counts, material aging, weld condition, and temperature-dependent material properties instead of relying exclusively on nominal design information. Periodic ultrasonic thickness measurement, weld inspection, hardness assessment, metallographic evaluation, and appropriate nondestructive examination should be integrated with updated finite element models to improve component-specific life estimates. The optimization framework should also be reapplied after major operational changes, repair welding, material replacement, evidence of accelerated wall thinning, or significant changes in cycling frequency. Statistical sensitivity and uncertainty analysis should accompany finite element assessment so that the effects of uncertain material properties, thermal boundary conditions, operating histories, and inspection measurements can be quantified before maintenance or continued-service decisions are made. Finally, optimized operating parameters should be verified against applicable boiler and pressure-vessel design requirements, inspection criteria, and plant-specific safety constraints before implementation. Through coordinated use of condition monitoring, validated thermomechanical simulation, controlled operating practices, targeted geometric improvement, and periodic remaining-life reassessment, industrial facilities can reduce avoidable creep-fatigue accumulation, prioritize maintenance resources toward the most critical locations, and support safer and more technically justified extension of boiler pressure-component service life.

LIMITATIONS

This study had several limitations that should be considered when interpreting the thermomechanical optimization and remaining-service-life results. First, the investigation was based primarily on finite element simulations of 216 representative component models and 1,296 thermomechanical cases; therefore, the calculated temperature fields, stresses, strains, creep-fatigue damage, and remaining-life estimates depended on the accuracy of the adopted geometry, material properties, constitutive relationships, boundary conditions, and operating histories. Although numerical validation produced strong agreement with reference data and principal deviations remained below 5%, finite element models could not reproduce every physical irregularity present in operating industrial boilers. Local manufacturing tolerances, surface imperfections, residual stresses, weld defects, microstructural heterogeneity, oxidation, corrosion morphology, and complex support interactions were necessarily simplified in some configurations. Second, temperature-dependent material properties were incorporated, but complete component-specific material characterization was not available for every simulated service condition. Service-aged materials can exhibit considerable spatial variability in creep strength, fatigue resistance, hardness, fracture behavior, and thermal properties because degradation depends on local temperature exposure, metallurgical history, repairs, and previous loading. Third, wall thinning was represented using measured or assumed thickness-loss conditions, whereas actual corrosion, erosion, and flow-accelerated corrosion may produce irregular three-dimensional defect geometries that generate more complex local stresses than uniform or parameterized thinning. Fourth, historical pressure and temperature conditions were reconstructed using available operational information; consequently, short-duration temperature excursions, undocumented overloads, unrecorded shutdown events, and local thermal disturbances might not have been completely represented.

REFERENCES

[1]. Afangide, E., Sinha, J. K., & Katnam, K. (2018). Quantified approach to pipeline health and integrity management. *Journal of Loss Prevention in the Process Industries*, *54*, 28-36.

[2]. Animah, I., & Shafiee, M. (2018). Condition assessment, remaining useful life prediction and life extension decision making for offshore oil and gas assets. *Journal of Loss Prevention in the Process Industries*, *53*, 17-28.

[3]. Ashik, M., & Shabbir, A. (2022). Digital Twin-Enabled Predictive Maintenance for Rotating and Static Equipment: Bridging FEA-Based Failure Analysis with Real-Time Asset Health Monitoring in Energy and Power Facilities. *International Journal of Scientific Interdisciplinary Research*, *12*(05), 01–37. https://doi.org/10.63125/0qaysz49

[4]. Assefinejad, A., Kermanpur, A., Eslami, A., & Kangazian, J. (2020). Failure investigation of water wall tubes in a drum boiler of a thermal power plant. *Engineering Failure Analysis*, *118*, 104869.

[5]. Bartošák, M., Horvath, J., & Španiel, M. (2020). Isothermal low-cycle fatigue and fatigue-creep of a 42CrMo4 steel. *International Journal of Fatigue*, *135*, 105538.

[6]. Belhocine, A., & Abdullah, O. I. (2020). Thermomechanical model for the analysis of disc brake using the finite element method in frictional contact. *Multiscale Science and Engineering*, *2*(1), 27-41.

[7]. Berto, F. (2016). Fatigue and fracture assessment of notched components by means of the Strain Energy Density. *Engineering Fracture Mechanics*, *167*, 176-187.

[8]. Di Bari, R., Belleri, A., Marini, A., Horn, R., & Gantner, J. (2020). Probabilistic life-cycle assessment of service life extension on renovated buildings under seismic hazard. *Buildings*, *10*(3), 48.

[9]. dos Santos, F. F. M., Furtado, H. C., & de Almeida, L. H. (2018). Remaining life evaluation based on strain deformation monitoring. *Journal of Failure Analysis and Prevention*, *18*(4), 809-818.

[10]. Duda, P. (2016). Inverse estimation of the transient-state stress distribution in the power boiler pressure components. *International Journal of Mechanical Sciences*, *107*, 201-214.

[11]. Duda, P., & Konieczny, M. (2019). A new algorithm for solving an inverse transient heat conduction problem by dividing a complex domain into parts. *International Journal of Heat and Mass Transfer*, *128*, 865-874.

[12]. Dundulis, G., Žutautaitė, I., Janulionis, R., Ušpuras, E., Rimkevičius, S., & Eid, M. (2016). Integrated failure probability estimation based on structural integrity analysis and failure data: Natural gas pipeline case. *Reliability Engineering & System Safety*, *156*, 195-202.

[13]. Fan, K., Li, D., Li, L.-y., & Wu, J. (2019). Effect of temperature gradient on transient thermal creep of heated and stressed concrete in transient state tests. *Construction and Building Materials*, *222*, 839-851.

[14]. Fan, X., Kuhn, B., Pöpperlová, J., Bleck, W., & Krupp, U. (2020). Thermomechanically induced precipitation in high-performance ferritic (HiperFer) stainless steels. *Applied Sciences*, *10*(16), 5713.

[15]. Fathalla, E., Tanaka, Y., & Maekawa, K. (2018). Remaining fatigue life assessment of in-service road bridge decks based upon artificial neural networks. *Engineering Structures*, *171*, 602-616.

[16]. Fathalla, E., Tanaka, Y., Maekawa, K., & Sakurai, A. (2018). Quantitative deterioration assessment of road bridge decks based on site inspected cracks. *Applied Sciences*, *8*(7), 1197.

[17]. Fischer, T., & Kuhn, B. (2019). Impact of frequency, hold time and atmosphere on creep-fatigue of a 9–12% Cr steel from 300° C− 600° C. *International Journal of Fatigue*, *124*, 288-302.

[18]. Fu, H., Wang, W., Chen, X., Pia, G., & Li, J. (2020). Grain boundary design based on fractal theory to improve intergranular corrosion resistance of TWIP steels. *Materials & Design*, *185*, 108253.

[19]. Furrer, D. U., Dimiduk, D. M., Cotton, J. D., & Ward, C. H. (2017). Making the case for a model-based definition of engineering materials. *Integrating Materials and Manufacturing Innovation*, *6*(3), 249-263.

[20]. Goyal, S., Mariappan, K., Shankar, V., Sandhya, R., Laha, K., & Bhaduri, A. (2018). Studies on creep-fatigue interaction behaviour of Alloy 617M. *Materials Science and Engineering: A*, *730*, 16-23.

[21]. Guglielmino, E., Pino, R., Servetto, C., & Sili, A. (2016). Creep damage of high alloyed reformer tubes. In *Handbook of materials failure analysis with case studies from the chemicals, concrete and power industries* (pp. 69-91). Elsevier.

[22]. Hanifi, H., Pander, M., Zeller, U., Ilse, K., Dassler, D., Mirza, M., Bahattab, M. A., Jaeckel, B., Hagendorf, C., & Ebert, M. (2020). Loss analysis and optimization of PV module components and design to achieve higher energy yield and longer service life in desert regions. *Applied energy*, *280*, 116028.

[23]. Haq, M., Bhalla, S., & Naqvi, T. (2020). Fatigue damage and residual fatigue life assessment in reinforced concrete frames using PZT-impedance transducers. *Cement and Concrete Composites*, *114*, 103771.

[24]. Harris, M., Potgieter, J., Archer, R., & Arif, K. M. (2019). Effect of material and process specific factors on the strength of printed parts in fused filament fabrication: A review of recent developments. *Materials*, *12*(10), 1664.

[25]. Hobbacher, A., & Baumgartner, J. (2016). *Recommendations for fatigue design of welded joints and components* (Vol. 47). Springer.

[26]. Honarmandi, P., & Arróyave, R. (2020). Uncertainty quantification and propagation in computational materials science and simulation-assisted materials design. *Integrating Materials and Manufacturing Innovation*, *9*(1), 103-143.

[27]. Hou, A., Jin, S., Harmuth, H., & Gruber, D. (2018). A Method for Steel Ladle Lining Optimization Applying Thermomechanical Modeling and Taguchi Approaches: Hou, Jin, Harmuth, and Gruber. *Jom*, *70*(11), 2449-2456.

[28]. Hu, Z., & Mahadevan, S. (2017). Uncertainty quantification and management in additive manufacturing: current status, needs, and opportunities. *The International Journal of Advanced Manufacturing Technology*, *93*(5), 2855-2874.

[29]. Jiang, Y., Li, C., Di, X., Wang, D., & Liu, J. (2020). EBSD analysis of microstructures and mechanical properties of softened zones in X60 reeled-pipeline welded joint after cyclic plastic deformation. *Welding in the World*, *64*(7), 1213-1225.

[30]. Jiao, J., De, X., Chen, Z., & Zhao, T. (2019). Integrated circuit failure analysis and reliability prediction based on physics of failure. *Engineering Failure Analysis*, *104*, 714-726.

[31]. Ju, Y., Liu, J., Liu, H., Tian, K., & Ge, Z. (2016). On the thermal spalling mechanism of reactive powder concrete exposed to high temperature: Numerical and experimental studies. *International Journal of Heat and Mass Transfer*, *98*, 493-507.

[32]. Kapadia, P., Davies, C., Pirling, T., Hofmann, M., Wimpory, R., Hosseinzadeh, F., Dean, D., & Nikbin, K. (2017). Quantification of residual stresses in electron beam welded fracture mechanics specimens. *International journal of solids and structures*, *106*, 106-118.

[33]. Kazi Rakib Hasan, S., & Adnan, S. (2022). Quantitative Assessment of Machine Learning-Based Schedule Risk Prediction for Reducing Delays in Complex Technology Projects. *Review of Applied Science and Technology*, *1*(04), 464–501. https://doi.org/10.63125/dn8nkm85

[34]. Khorsand, M., & Tang, Y. (2018). On the qualitative dynamics of rotating disks: Thermal shocks and structural integrity. *International Journal of Pressure Vessels and Piping*, *166*, 35-47.

[35]. Kim, J.-S., Kim, M.-W., & Yang, J.-S. (2020). Investigation on effect of thermal aging embrittlement on residual stresses of austenitic stainless steel repair welds in nuclear components subject to seismic loads. *Journal of Mechanical Science and Technology*, *34*(7), 2821-2831.

[36]. Kim, Y.-S., Kim, W.-C., & Kim, J.-G. (2019). Bulging rupture and caustic corrosion of a boiler tube in a thermal power plant. *Engineering Failure Analysis*, *104*, 560-567.

[37]. Klimiec, E., Kaczmarek, H., Królikowski, B., & Kołaszczyński, G. (2020). Cellular polyolefin composites as piezoelectric materials: properties and applications. *Polymers*, *12*(11), 2698.

[38]. Kotha, S., Ozturk, D., Smarslok, B., & Ghosh, S. (2020). Uncertainty quantified parametrically homogenized constitutive models for microstructure-integrated structural simulations. *Integrating Materials and Manufacturing Innovation*, *9*(4), 322-338.

[39]. Kumar, M. M., Joshna, K., Markendeya, R., & Rawat, M. (2016). Effect of steamside oxidation and fireside corrosion degradation processes on creep life of service exposed boiler tubes. *International Journal of Pressure Vessels and Piping*, *144*, 45-48.

[40]. Létal, T., Turek, V., Babička Fialová, D., & Jegla, Z. (2020). Nonlinear finite element analysis-based flow distribution and heat transfer model. *Energies*, *13*(7), 1664.

[41]. Li, D.-H., Shang, D.-G., Zhang, C.-C., Liu, X.-D., Li, F.-D., & Li, Z.-G. (2018). Thermo-mechanical fatigue damage behavior for Ni-based superalloy under axial-torsional loading. *Materials Science and Engineering: A*, *719*, 61-71.

[42]. Li, M., Benaarbia, A., Morris, A., & Sun, W. (2020). Assessment of potential service-life performance for MarBN steel power plant header under flexible thermomechanical operations. *International Journal of Fatigue*, *135*, 105565.

[43]. Liu, J., Gaynor, A. T., Chen, S., Kang, Z., Suresh, K., Takezawa, A., Li, L., Kato, J., Tang, J., & Wang, C. C. (2018). Current and future trends in topology optimization for additive manufacturing: J. Liu et al. *Structural and multidisciplinary optimization*, *57*(6), 2457-2483.

[44]. Liu, Q., Zhang, P., Cheng, S., Niu, J., & Liu, D. (2016). Heat transfer and thermo-elastic analysis of copper steel composite stave. *International Journal of Heat and Mass Transfer*, *103*, 341-348.

[45]. Lyubimova, L. L., Tashlykov, A. A., Tabakaev, R. B., Levin, A. A., & Popov, A. Y. (2017). The effect of thermo-mechanical loading on fracture-related parameters of austenitic steel. *Engineering Failure Analysis*, *81*, 45-56.

[46]. Mahbubul, I., Mahmudul, I., Shifa, T., Mahfuza, T., & Shima Ali, S. (2022). Exploring The Potential of Visual Narratives and Interactive Gamified Communication Systems to Prevent Disease, Counter Health Misinformation, And Strengthen Public Trust in Low-Literacy Communities: A Literature Review. *American Journal of Interdisciplinary Studies*, *3*(02), 165-220. https://doi.org/10.63125/zmqs4n64

[47]. Mashayekhi, M., & Santini-Bell, E. (2020). Fatigue assessment of a complex welded steel bridge connection utilizing a three-dimensional multi-scale finite element model and hotspot stress method. *Engineering Structures*, *214*, 110624.

[48]. Mashfiqur, R., & Md, A. (2022). Monte Carlo Simulation and Stochastic Cash-Flow Modeling for Reducing Liquidity Risk in Project-Based Enterprises. *International Journal of Scientific Interdisciplinary Research*, *1*(01), 382–431. https://doi.org/10.63125/zf3fwv21

[49]. Mashiat, N., & Md Anisur Rahman, M. (2022). Machine Learning Approaches to Credit Risk Scoring and Default Prediction in Small-Business Lending: Empirical Evidence from Lending Portfolio Data. *American Journal of Data Science and Analytics*, *3*(06), 137-182. https://doi.org/10.63125/j256rs96

[50]. Md, A., & Gazi Yeasin, A. (2022). Machine Learning Enhanced Spatial-Data Workflow Redesign: A Quantitative Evaluation of Task Success and Operational Cost Reduction in Enterprise LiDAR Platforms. *American Journal of Data Science and Analytics*, *3*(06), 80-136. https://doi.org/10.63125/0den7c02

[51]. Md Ashfaq, S., & Abdullah Mohammad, S. (2022). CNT/PANI Composite Electrodes for Flexible Fiber-Shaped Dye-Sensitized Solar Cells: Synthesis, Characterization, and Photovoltaic Performance. *American Journal of Interdisciplinary Studies*, *3*(02), 221-274. https://doi.org/10.63125/m334mf41

[52]. Megahed, M., Mindt, H.-W., N'Dri, N., Duan, H., & Desmaison, O. (2016). Metal additive-manufacturing process and residual stress modeling. *Integrating Materials and Manufacturing Innovation*, *5*(1), 61-93.

[53]. Mey-Cloutier, S., Caliot, C., Kribus, A., Gray, Y., & Flamant, G. (2016). Experimental study of ceramic foams used as high temperature volumetric solar absorber. *Solar Energy*, *136*, 226-235.

[54]. Moussavi Torshizi, S. E., & Jahangiri, A. (2018). Analysis of fatigue–creep crack growth in the superheater header of a power plant boilers and estimation of its remaining lifetime. *Journal of Failure Analysis and Prevention*, *18*(1), 189-198.

[55]. Mst Kaniz, F., & Jahanara, A. (2022). Lean Six Sigma Implementation in Home Health Administrative Operations: A DMAIC Case Study of Managerial Workflow Redesign and Error Reduction. *International Journal of Scientific Interdisciplinary Research*, *12*(04), 01–60. https://doi.org/10.63125/xchca204

[56]. Muránsky, O., Hosseinzadeh, F., Hamelin, C., Traore, Y., & Bendeich, P. (2018). Investigating optimal cutting configurations for the contour method of weld residual stress measurement. *International Journal of Pressure Vessels and Piping*, *164*, 55-67.

[57]. Murmura, M., & Annesini, M. (2020). Methodologies for the design of solar receiver/reactors for thermochemical hydrogen production. *Processes*, *8*(3), 308.

[58]. Musa, I. A., Mashiri, F. R., Zhu, X., & Tong, L. (2018). Experimental stress concentration factor in concrete-filled steel tubular T-joints. *Journal of Constructional Steel Research*, *150*, 442-451.
[59]. Najjar, Y. S., Alalul, O. F., & Abu-Shamleh, A. (2020). Steam turbine bottoming cycle deterioration under different load conditions. *Thermal Science and Engineering Progress*, *20*, 100733.
[60]. Nykyforchyn, H., Krechkovska, H., Student, O., & Zvirko, O. (2019). Feature of stress corrosion cracking of degraded gas pipeline steels. *Procedia Structural Integrity*, *16*, 153-160.
[61]. Omar, T., & Nehdi, M. L. (2018). Condition assessment of reinforced concrete bridges: Current practice and research challenges. *Infrastructures*, *3*(3), 36.
[62]. Papaelias, M., Cheng, L., Kogia, M., Mohimi, A., Kappatos, V., Selcuk, C., Constantinou, L., Muñoz, C. Q. G., Marquez, F. P. G., & Gan, T.-H. (2016). Inspection and structural health monitoring techniques for concentrated solar power plants. *Renewable Energy*, *85*, 1178-1191.
[63]. Pástor, M., Lengvarský, P., Trebuňa, F., & Čarák, P. (2020). Prediction of failures in steam boiler using quantification of residual stresses. *Engineering Failure Analysis*, *118*, 104808.
[64]. Pilarczyk, M., Węglowski, B., & Nord, L. O. (2019). A comprehensive thermal and structural transient analysis of a boiler's steam outlet header by means of a dedicated algorithm and FEM simulation. *Energies*, *13*(1), 111.
[65]. Porter, T., Findley, K., Kaufman, M., & Wright, R. (2019). Assessment of creep-fatigue behavior, deformation mechanisms, and microstructural evolution of alloy 709 under accelerated conditions. *International Journal of Fatigue*, *124*, 205-216.
[66]. Prakash, P. R., Azenha, M., Pereira, J. M., & Lourenço, P. B. (2020). Finite element based micro modelling of masonry walls subjected to fire exposure: Framework validation and structural implications. *Engineering Structures*, *213*, 110545.
[67]. Qazi, M. I., Akhtar, R., Abas, M., Khalid, Q. S., Babar, A. R., & Pruncu, C. I. (2020). An integrated approach of GRA coupled with principal component analysis for multi-optimization of shielded metal arc welding (SMAW) process. *Materials*, *13*(16), 3457.
[68]. Ray, A., Roy, N., Raj, A., & Roy, B. (2016). Structural integrity of service exposed primary reformer tube in a petrochemical industry. *International Journal of Pressure Vessels and Piping*, *137*, 46-57.
[69]. Rizk, G., Legrand, V., Khalil, K., Casari, P., & Jacquemin, F. (2018). Durability of sandwich composites under extreme conditions: Towards the prediction of fire resistance properties based on thermo-mechanical measurements. *Composite Structures*, *186*, 233-245.
[70]. Romanowicz, P. J., Szybiński, B., & Wygoda, M. (2020). Application of DIC method in the analysis of stress concentration and plastic zone development problems. *Materials*, *13*(16), 3460.
[71]. Rouse, J., Hyde, C., & Morris, A. (2018). A neural network approach for determining spatial and geometry dependent Green's functions for thermal stress approximation in power plant header components. *International Journal of Pressure Vessels and Piping*, *168*, 269-288.
[72]. Rui, J., Xiaofan, H., & Yuhai, L. (2018). Individual aircraft life monitoring: An engineering approach for fatigue damage evaluation. *Chinese Journal of Aeronautics*, *31*(4), 727-739.
[73]. Saad, D., Dundulis, G., & Janulionis, R. (2019). Numerical simulation of SIF in Es-Salam research reactor vessel. *Engineering Failure Analysis*, *96*, 394-408.
[74]. Sadia, Z., & Maishar Mostari, Z. (2022). The Impact of Interactive Dashboard Visualization on Data-Driven Decision Making in Financial Services: A Qualitative Evaluation. *International Journal of Scientific Interdisciplinary Research*, *12*(03), 01–35. https://doi.org/10.63125/3jstsv75
[75]. Sairajan, K., Aglietti, G., & Mani, K. (2016). A review of multifunctional structure technology for aerospace applications. *Acta astronautica*, *120*, 30-42.
[76]. Salifu, S., Desai, D., & Kok, S. (2020). Creep–fatigue interaction of P91 steam piping subjected to typical start-up and shutdown cycles. *Journal of Failure Analysis and Prevention*, *20*(3), 1055-1064.
[77]. Sarkar, S., Singh, I. V., & Mishra, B. (2020). A Thermo-mechanical gradient enhanced damage method for fracture. *Computational Mechanics*, *66*(6), 1399-1426.
[78]. Schiro, F., Stoppato, A., & Benato, A. (2020). Modelling and analyzing the impact of hydrogen enriched natural gas on domestic gas boilers in a decarbonization perspective. *Carbon resources conversion*, *3*, 122-129.
[79]. Sekar, K., Gupta, M., & Arockiarajan, A. (2019). Advances In Manufacturing Processes. In (Vol. 413, pp. 0): Springer.
[80]. Ševeček, M., Gurgen, A., Seshadri, A., Che, Y., Wagih, M., Phillips, B., Champagne, V., & Shirvan, K. (2018). Development of Cr cold spray–coated fuel cladding with enhanced accident tolerance. *Nuclear Engineering and Technology*, *50*(2), 229-236.
[81]. Shabani, A., Kioumarsi, M., Plevris, V., & Stamatopoulos, H. (2020). Structural vulnerability assessment of heritage timber buildings: A methodological proposal. *Forests*, *11*(8), 881.
[82]. Shaiful, M., Anisur, R., & Md, A. (2022). A Systematic Literature Review on the Role of Digital Health Twins in Preventive Healthcare For Personal and Corporate Wellbeing. *American Journal of Interdisciplinary Studies*, *3*(04), 1-31. https://doi.org/10.63125/negjw373
[83]. Shankar, V., Mariappan, K., Sandhya, R., Laha, K., & Bhaduri, A. (2017). Long term creep-fatigue interaction studies on India-specific reduced activation ferritic-martensitic (IN-RAFM) steel. *International Journal of Fatigue*, *98*, 259-268.
[84]. Shetty, N., Livitsanos, G., Van Roy, N., Aggelis, D. G., Van Hemelrijck, D., Wevers, M., & Verstrynge, E. (2019). Quantification of progressive structural integrity loss in masonry with Acoustic Emission-based damage classification. *Construction and Building Materials*, *194*, 192-204.

[85]. Singh, U., Shrivastav, V., & Sen, R. (2020). Life Estimation Strategy for a Nuclear Reactor Pressure Vessel. In *Fatigue, Durability, and Fracture Mechanics: Proceedings of Fatigue Durability India 2019* (pp. 31-51). Springer.

[86]. Souza, J., Silva, A., de Brito, J., & Bauer, E. (2018). Analysis of the influencing factors of external wall ceramic claddings' service life using regression techniques. *Engineering Failure Analysis*, *83*, 141-155.

[87]. Stabak, D., & Md Shahid, N. (2022). Empirical Assessment of Uncertainty-Aware Real-Time Decision-Making for Reliable and Resilient Cyber-Physical Systems. *International Journal of Scientific Interdisciplinary Research*, *1*(01), 432–477. https://doi.org/10.63125/q3r4kk16

[88]. Sun, J., & Yuan, H. (2019). Cyclic plasticity modeling of nickel-based superalloy Inconel 718 under multi-axial thermo-mechanical fatigue loading conditions. *International Journal of Fatigue*, *119*, 89-101.

[89]. Syed Feroz, A., & Md Mahamud Pervaz, P. (2022). Root-Cause Analysis and FMEA-Driven Reliability Improvement in Gas Production Facilities: A Multi-Year Empirical Study. *International Journal of Scientific Interdisciplinary Research*, *12*(10), 01–53. https://doi.org/10.63125/70msp878

[90]. Tahir, F., Dahire, S., & Liu, Y. (2017). Image-based creep-fatigue damage mechanism investigation of Alloy 617 at 950° C. *Materials Science and Engineering: A*, *679*, 391-400.

[91]. Tognoli, M., Najafi, B., Marchesi, R., & Rinaldi, F. (2019). Dynamic modelling, experimental validation, and thermo-economic analysis of industrial fire-tube boilers with stagnation point reverse flow combustor. *Applied Thermal Engineering*, *149*, 1394-1407.

[92]. Tognoli, M., Najafi, B., & Rinaldi, F. (2018). Dynamic modelling and optimal sizing of industrial fire-tube boilers for various demand profiles. *Applied Thermal Engineering*, *132*, 341-351.

[93]. Trampus, P. (2019). Role and importance of NDE in nuclear power plant life extension. *Procedia Structural Integrity*, *16*, 161-168.

[94]. Trzepieciński, T. (2020). Recent developments and trends in sheet metal forming. *Metals*, *10*(6), 779.

[95]. Tsanakas, J. A., Ha, L., & Buerhop, C. (2016). Faults and infrared thermographic diagnosis in operating c-Si photovoltaic modules: A review of research and future challenges. *Renewable and sustainable energy reviews*, *62*, 695-709.

[96]. Van Rooyen, M., Becker, T., Westraadt, J., & Marx, G. (2019). Creep damage assessment of ex-service 12% Cr power plant steel using digital image correlation and quantitative microstructural evaluation. *Materials*, *12*(19), 3106.

[97]. Venkatesh, V., Green, R., O'Connell, J., Cernatescu, I., Goetz, R., Wong, T., Streich, B., Saraf, V., Glavicic, M., & Slavik, D. (2018). An ICME framework for incorporating bulk residual stresses in rotor component design. *Integrating Materials and Manufacturing Innovation*, *7*(4), 173-185.

[98]. Verstrynge, E., De Wilder, K., Drougkas, A., Voet, E., Van Balen, K., & Wevers, M. (2018). Crack monitoring in historical masonry with distributed strain and acoustic emission sensing techniques. *Construction and Building Materials*, *162*, 898-907.

[99]. Wang, H., Xu, S., Li, A., & Kang, K. (2018). Experimental and numerical investigation on seismic performance of corroded welded steel connections. *Engineering Structures*, *174*, 10-25.

[100]. Wang, M., Pang, J., Zhang, M., Liu, H., Li, S., & Zhang, Z. (2018). Thermo-mechanical fatigue behavior and life prediction of the Al-Si piston alloy. *Materials Science and Engineering: A*, *715*, 62-72.

[101]. Wang, R.-Z., Zhu, S.-P., Wang, J., Zhang, X.-C., Tu, S.-T., & Zhang, C.-C. (2019). High temperature fatigue and creep-fatigue behaviors in a Ni-based superalloy: Damage mechanisms and life assessment. *International Journal of Fatigue*, *118*, 8-21.

[102]. Węglowski, B., & Pilarczyk, M. (2018). Experimental and numerical verification of transient spatial temperature distribution in thick-walled pressure components. *Journal of Mechanical Science and Technology*, *32*(3), 1087-1098.

[103]. Wei, X., Wen, Z., Xiao, L., & Wu, C. (2018). Review of fatigue assessment approaches for tubular joints in CFST trusses. *International Journal of Fatigue*, *113*, 43-53.

[104]. Xu, Z., & Zhu, J. (2020). Measurement of accumulated height of exfoliated oxide scales in austenitic boiler tubes using pulsed eddy current testing. *Russian Journal of Nondestructive Testing*, *56*(4), 350-360.

[105]. Ye, J., Wang, Y., Li, Z., Saafi, M., Jia, F., Huang, B., & Ye, J. (2020). Failure analysis of fiber-reinforced composites subjected to coupled thermo-mechanical loading. *Composite Structures*, *235*, 111756.

[106]. Yıldırım, H. C. (2017). Recent results on fatigue strength improvement of high-strength steel welded joints. *International Journal of Fatigue*, *101*, 408-420.

[107]. Zelmati, D., Bouledroua, O., Hafsi, Z., & Djukic, M. B. (2020). Probabilistic analysis of corroded pipeline under localized corrosion defects based on the intelligent inspection tool. *Engineering Failure Analysis*, *115*, 104683.

[108]. Zerbst, U., Madia, M., Schork, B., Hensel, J., Kucharczyk, P., Ngoula, D., Tchuindjang, D., Bernhard, J., & Beckmann, C. (2018). Fatigue and fracture of weldments. In *Fatigue and Fracture of Weldments: The IBESS Approach for the Determination of the Fatigue Life and Strength of Weldments by Fracture Mechanics Analysis* (pp. 1-130). Springer.

[109]. Zhang, J., Li, X., Xu, D., & Yang, R. (2019). Recent progress in the simulation of microstructure evolution in titanium alloys. *Progress in Natural Science: Materials International*, *29*(3), 295-304.

[110]. Zhang, T., Wang, X., Zhang, W., Hassan, T., & Gong, J. (2020). Fatigue–creep interaction of P92 steel and modified constitutive modelling for simulation of the responses. *Metals*, *10*(3), 307.

[111]. Zhang, Z., Feng, Y., Tan, Q., Zou, J., Li, J., Zhou, X., Sun, G., & Wang, Y. (2019). Residual stress distribution in Ni-based superalloy turbine discs during fabrication evaluated by neutron/X-ray diffraction measurement and thermomechanical simulation. *Materials & Design*, *166*, 107603.